Marine and Petroleum Geology 79 (2017) 300–320

Contents lists available at ScienceDirect

Marine and Petroleum Geology

journal homepage: www.elsevier.com/locate/marpetgeo

Research paper

An incomplete correlation between pre-salt topography, top reservoir erosion, and salt deformation in deep-water Santos Basin (SE Brazil)

Tiago M. Alves [a, *], Marcos Fetter [b], Cláudio Lima [b], Joseph A. Cartwright [c], John Cosgrove [d], Adriana Gangá [b], Cláudia L. Queiroz [b], Michael Strugale [b]

[a] 3D Seismic Lab – School of Earth and Ocean Sciences, Cardiff University – Main Building, Park Place, Cardiff, CF10 3AT, United Kingdom
[b] Petrobras-E&P, Av. República do Chile 65, Rio de Janeiro, 20031-912 Brazil
[c] Shell Geosciences Laboratory, Department of Earth Sciences, University of Oxford, South Parks Road, Oxford, OX1 3AN, United Kingdom
[d] Department of Earth Science & Engineering, Imperial College of London, Royal School of Mines, Prince Consort Road, Imperial College London, SW7 2BP, United Kingdom

ARTICLE INFO

Article history:
Received 4 November 2014
Received in revised form
13 July 2016
Accepted 17 October 2016
Available online 20 October 2016

Keywords:
Continental margins
SE Brazil
Fold-and-thrust belts
Pre-salt reservoirs
Erosion
Tectonic reactivation

ABSTRACT

In deep-water Santos Basin, SE Brazil, hypersaline conditions during the Aptian resulted in the accumulation of halite and carnallite over which stratified evaporites, carbonates and shales were folded, translated downslope and thrusted above syn-rift structures. As a result, high-quality 3D seismic data reveal an incomplete relationship between pre-salt topography and the development of folds and thrusts in Aptian salt and younger units. In the study area, three characteristics contrast with known postulates on passive margins' fold-and-thrust belts: a) the largest thrusts do not necessarily occur where the salt is thicker, b) synthetic-to-antithetic fault ratios are atypically high on the distal margin, and c) regions of intense folding do not necessarily coincide with the position of the larger syn-rift horsts and ramps below the salt. Regions marked by important erosion and truncation of pre-salt strata, uplifted and exposed sub-aerially before the deposition of Aptian salt, can form structural lows at present or be part of horsts uplifted after the Aptian. This is an observation that suggests significant intra-salt shear drag above pre-salt structural highs during Aptian-Late Cretaceous gravitational gliding, but not on younger horsts and ramps reactivated after the main phase of salt movement. Either formed by drag or sub-aerial erosion, strata truncation below the Aptian salt does not correlate with the present-day pre-salt structure in terms of its magnitude and distribution. In addition, there is a marked increase in deformation towards the distal margin, where low-angle thrusts are ubiquitous on seismic data. The geometry and large synthetic-to-antithetic fault ratios of post-salt strata on the distal margin lead us to consider a combination of gravitational gliding of salt from the northwest and ridge push from the east as responsible for the observed styles of salt deformation.

1. Introduction

The relative magnitude of deformation in fold-and-thrust belts depends on the physical properties of the upper crust, its thickness, local deformation effects and the type of basal décollement (Ruh et al., 2012; Tavani et al., 2015). Secondary processes controlling deformation in these belts include: a) variable fluid-induced stresses in what is, essentially, a porous medium, b) cohesive forces in deformed strata, c) distinct geometries and rheological properties of strata at the basal décollement(s), d) thermal variations, normally occurring in association with igneous episodes; e) variable roughness of oceanic plates in the form of subducted oceanic features, and f) the presence of inherited syn-rift topography capable of localising deformation during the early compressional stages (Moore et al., 2001; Henry et al., 2002; Bangs et al., 2004; Kodaira et al., 2004; Bilotti and Shaw, 2005; Peacock et al., 2005; Fuller et al., 2006; Bangs et al., 2006; Morley et al., 2011; Rowan, 2014).

On convergent margins, for constant basal dip and uniform material strength, an accretionary wedge at the point of failure will transition to contraction where the taper angle changes or friction at the basal décollement increases (Davis et al., 1983). However, fold-and-thrust belts of passive margins such as SE Brazil's are associated with gravitational collapse over thick evaporite and shale units (Fig. 1), presenting characteristics that differ from

* Corresponding author.
E-mail address: alvest@cardiff.ac.uk (T.M. Alves).

http://dx.doi.org/10.1016/j.marpetgeo.2016.10.015

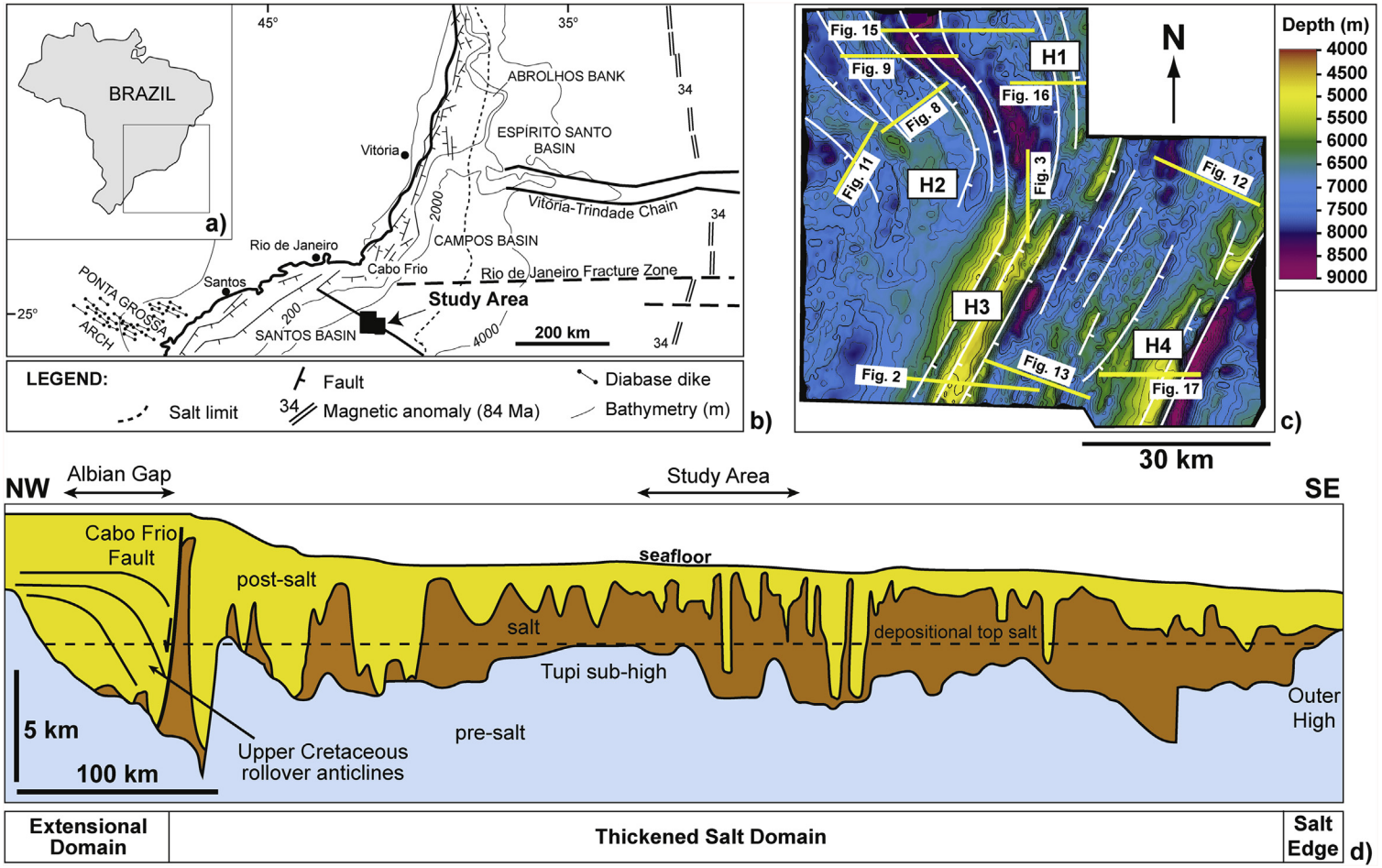

Fig. 1. a) Map of the Southeast Brazilian margin showing the location of the Santos, Campos and Espírito Santo basins in relation to main fault zones. b) Location of the interpreted 3D seismic volume on the SE Brazilian margin. c) Structural map of the base syn-rift succession (Horizon S1) highlighting the location of structural highs H1 to H4, adjacent syn-rift depocentres and structural highs. Main faults are marked in white colour, and interpreted seismic lines in yellow. d) Simplified section across the central Santos Basin showing the geometry of Aptian evaporites in relation to salt-related structural domains (modified from Davison et al., 2012; Jackson et al., 2015). The location of the section is shown in b). (For interpretation of the references to colour in this figure legend, the reader is referred to the web version of this article.)

accretionary wedges on convergent margins (Brun and Fort, 2011, 2012; Rowan et al., 2004; Albertz et al., 2010; Albertz and Ings, 2012). First, net shortening and deformation rates on passive margins are smaller than in collisional fold-and-thrust belts because the driving forces are weaker than those induced by lithospheric plate motions. Second, structural styles in passive-margin belts vary depending largely on the nature of the décollement layer, not the forces driving deformation (Rowan et al., 2000). As a result, fold-and-thrust belts on passive margins show a prevalence of oceanward-verging thrust anticlines if the basal décollement is composed of shales, and low synthetic-to-antithetic fault ratios in the presence of thick basal halite, i.e. faults often verge opposite to the shear sense at basal décollements comprising halite (Rowan et al., 2000, 2004; 2012). This means that frictional décollements result in asymmetric fault imbricates, whereas viscous décollements produce symmetrical folds with minor faulting of their limbs (Cotton and Koyi, 2000; Gemmer et al., 2005; Rowan et al., 2004; Ruh et al., 2012). Still to understand, however, is the effect of variable sub-décollement topography on kilometre-thick masses of salt or shale, and the degree of tectonic truncation in underlying strata that results from the gravitational gliding of such masses (see Billotti and Shaw, 2005; Brun and Fort, 2011; Rowan et al., 2012; Brun and Fort (2012) for discussions on the modes of salt tectonics on passive margins). In particular, the effect of shear stress gradients on the thrust geometry of post-salt units, and on underlying pre-salt strata, has not been investigated in SE Brazil, despite evidence of important erosion at top reservoir level (Davison, 2007). In the Santos Basin, Aptian salt moved downslope through a long distance over an important pre-salt reservoir interval composed of microbialites, tufas and limestones (Davison, 2007).

In salt units subject to gravitational instability, the effects of detachment dip are usually overlooked and considered to be cancelled out by the low shear resistance of salt (Koyi and Vendeville, 2003; Gemmer et al., 2005). Nevertheless, Dooley et al. (2007) and Rowan (2014) interpreted the vergence of fold-and-thrust belts to be stress balanced, and suggested that important perturbations to the base of gliding salt can bias vergence. These perturbations include pinch-outs, swells, scarps, faults and variations in salt thickness, which can be significantly enhanced by two key mechanisms. The first of these mechanisms considers tectonic shortening as capable to depress thrust blocks of overburden strata until they contact the base of salt, forming a weld. These same salt welds increase friction (or drag) at the base of moving salt. In the second mechanism, the overburden gravitational load can expel salt into diapirs, eventually extruding salt to the surface. Local thinning of salt increases frictional drag along the salt-sediment interface. As a result, Dooley et al. (2007) attributed variations in the geometry of salt-based thrust belts of passive margins to three main causes: a) low friction of the basal décollement, which favours near-symmetric pop-ups; b) the migration of mobile salt away from local loads created by overthrusting, thus reducing the seaward taper of the thrust belt, and c) shortening in gravity-driven systems, which quickly spreads to form wide thrust belts that are capable of overlap strain in time and space.

Recently, these concepts have been further developed to consider important drag in intra-, base- and top-salt surfaces of moving salt units (see page 957 and Fig. 12 in Weijermars et al., 2014). The latter authors stressed the presence of layer detachments within salt, a phenomenon often characterised by parallel stream lines. Salt creep promoted by gravity tectonics creates a lateral pressure gradient inside distinct salt sheets (Poiseuille flow) or moves the overburden sediments downslope (Couette flow). In both cases, particularly in mixed Poiseuille and Couette flows, drag forces increase with effective viscosity and velocity gradients in the creeping salt layer, particularly at the top-salt and base-salt surfaces. Weijermars et al. (2014) explained that the total shear stress near the stream-line boundaries consists of the shear stress contributions by the two different flow components, $T_{XY\ Couette}$ and $T_{XY\ Poiseuille}$, and proposed an analytical method to constrain the possible range (and spatial variations) in shear stress and drag on wellbores crossing creeping salt layers. These results complement Gemmer et al. (2005), who calculated the shear force of both Poiseuille and Couette flows. Poiseulle flow is directly proportional do the salt layer thickness, whereas the Couette flow was deemed inversely proportional to the thickness of the mobile unit (i.e., the thinner, the more drag).

This work focuses on the passive margin of SE Brazil, and constrains the history of folding of post-salt strata in deep-water Santos Basin (Fig. 1). We present new calculations of salt thickness and gradient(s) of basal ramps at pre-salt level to suggest that shear drag within thrusted and translated salt was an important phenomenon in the Santos Basin, SE Brazil (Fig. 1). These calculations are based on the fact that flow velocity and shear drag of the salt layer increase as salt moves across basement steps, i.e. where the viscous layer is effectively thinned as the cross-sectional area of the flow is reduced (Cotton and Koyi, 2000; Weijermars et al., 2014). Structural restorations across the Santos Basin suggest that Aptian salt was fully contained within its original depositional basin, with important post-depositional flow causing it to glide on the continental slope to be later expelled as salt nappes on transitional or oceanic crust (Davison et al., 2012) (Figs. 1d, 2 and 3).

The seismic sections in this paper show classic examples of thin-skinned folding and thrusting, combined with (or decoupled from) thick-skinned basement tectonics sensu Coward (1983). We will concentrate on characterising the effect of thick-skinned morphology and structure on the structural deformation of thin-skinned overburden translated above a moving evaporite layer. In summary, the scientific objectives of this paper are:

a) To understand the geometry of folded and thrusted salt sequences offshore SE Brazil;
b) To investigate the relationship between fold geometry and syn-rift structures at pre-salt level;
c) To understand the reactivation history of pre-salt successions based on the analysis of deformation in Aptian salt units.

In this paper, the geological setting of deep-water Santos Basin (SE Brazil) is presented first. Data and methods are then summarised, prior to a detailed structural analysis of pre-salt and post-salt units. The remaining sections address the significance of salt moving and ramping-up syn-rift structures, and the degree of erosion experienced by strata underneath the translated salt unit. At the end of the paper are discussed: a) the significance of the observed discrepancy between post-salt structures and the degree of erosion observed at pre-salt level and, b) ridge push as an additional controlling factor on salt deformation in distal parts of the Santos Basin. Throughout this paper the word ‘salt’, wherever deformation is described, refers to the mobile evaporitic layer, or lower evaporite unit in the seismic sections interpreted in this work, being mainly halite and carnallite (see Section 2). In addition, ‘halokinesis’ is defined as all processes associated with autonomous salt movements, with the main preconditioning factor for halokinetic processes being a heterogeneous (unstable) density stratification in the crust (Trusheim, 1957, 1960).

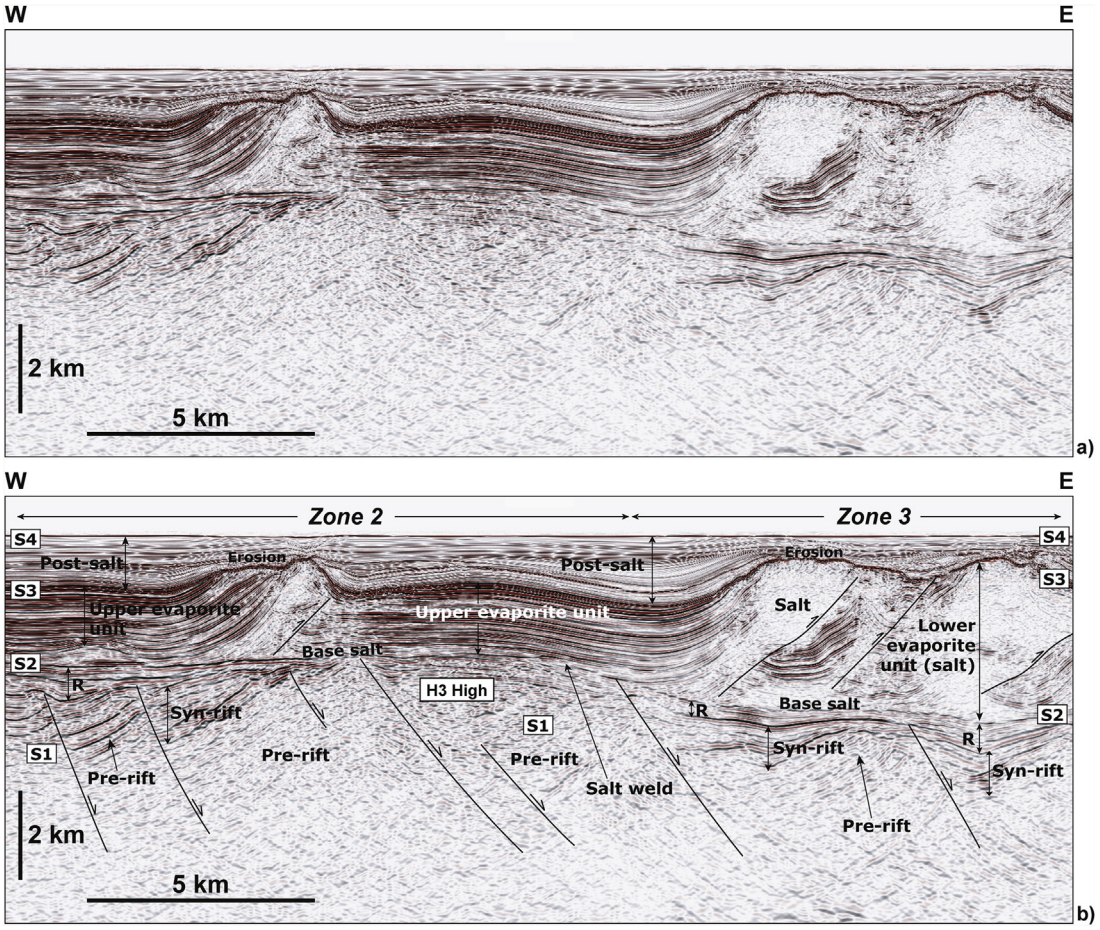

Fig. 2. Composite PSDM seismic line crossing structural high H3 (see Fig. 1c for relative location). The line shows developed faults bordering a series of half-grabens located to the east of H3. Note the significant erosion over H3 and the presence of developed syn-rift basin to the east of this same structure, i.e. in Zone 3. Main thrusts at salt level are highlighted together with the major normal faults crossing the pre-salt units.

2. Geological setting of SE Brazil

2.1. Syn-rift tectonic evolution of the Santos Basin

The study area is located on the lower continental slope of the Santos Basin, SE Brazil, in the thickened salt domain described in Davison et al. (2012) (Fig. 1b, 1d and 2). The interpreted seismic volume is located at the transition between a region of relatively thickened crust, where structural highs H1, H2 and H3 are observed, and an area to the east with significantly stretched (and thinned) continental crust (Figs. 1d, 2 and 3).

The Santos Basin was initially part of an extensive region of continental rifting separating South America and West Africa (Mohriak et al., 2008; Contreras et al., 2010; Davison et al., 2012) (Fig. 4). As a result, the study area records latest Jurassic-Early Cretaceous rifting, Late Cretaceous salt tectonics and multiple phases of tectonism related to the Andean Orogeny (Mégard, 1984; Gregory-Wodzicki, 2000; Lima, 2003). Continental breakup was triggered in the Austral Segment during the Late Jurassic and later propagated northwards into the equatorial segment (Bueno, 2004) (Fig. 4). Magnetic anomaly M0 (~125 Ma, Barremian-Aptian boundary; Gradstein et al., 2004), marks the opening of the South Atlantic Ocean at the Pan-African suture in the south and at the E–W segment of the São Francisco–Sangha cratons in the north (Aslanian et al., 2009; Moulin et al., 2010).

Following the onset of continental breakup, half-graben basins were first filled with non-marine strata of the Piçarras and Itapema Formations, and shallow-marine carbonates belonging to the Barra Velha Formation (Moreira et al., 2007), all part of the Guaratiba Group (Fig. 5). The Barra Velha Formation comprises the main pre-salt reservoir in deep-water areas of the Santos Basin. After the main syn-rift stage, a >2 km-thick evaporite succession was deposited in the study area (Ariri Formation; Moreira et al., 2007) (Fig. 4).

Borehole data from the Santos Basin indicate that Aptian salt is dominated by halite and carnallite in a lower autochthonous evaporite unit, whereas anhydrite, clastics and carbonates predominate in its upper part (Davison, 2007; Jackson et al., 2014). Davison et al. (2012) noted that evaporites in the Santos Basin were deposited relatively fast, with Freitas (2006) estimating a time span of 0.5 Ma for the accumulation of the entire salt succession. Importantly, the base salt was identified as comprising a smooth surface, with a small number of large faults producing offsets of up to 4 km at the base salt. In the study area, fault offsets of this magnitude are observed together with smaller faults and forced folds denoting a later stage of pre-salt tectonism (Figs. 2 and 3). This observation corroborates the interpretation in Davison et al. (2012), who state that fault scarp relief at the time of salt deposition was significantly less than the present-day offset at base salt.

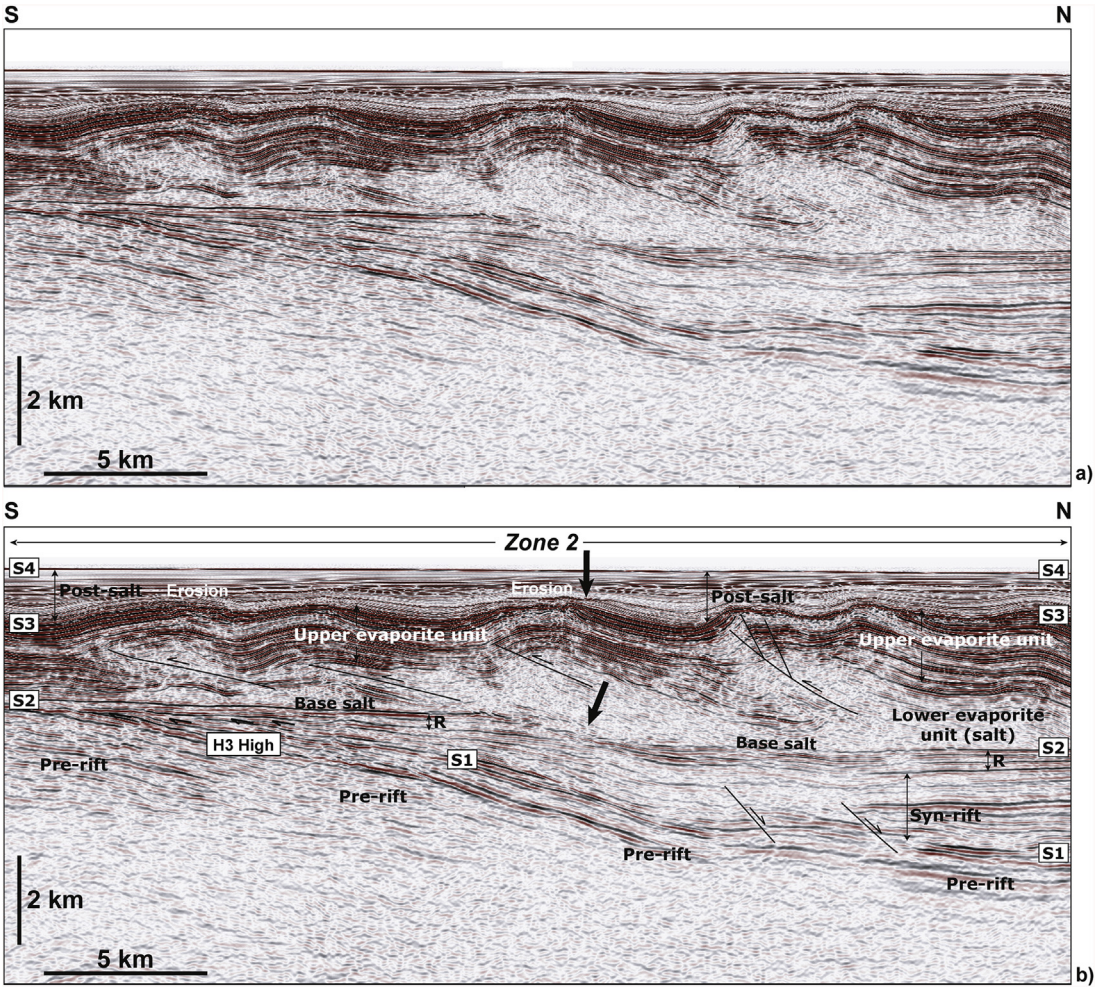

Fig. 3. Composite PSDM seismic line crossing structural high H3 from a N-S orientation. The line highlights a NW-SE erosional scarp that occurs north of the structural high H3 at top reservoir level. No significant fault occurs underneath the scarp, with this latter denoting erosion of a rising footwall block - in this paper suggested as partly induced by salt movement. Arrows indicate the regions where erosion is observed at the base and top of the Aptian salt.

2.2. Post-rift tectonic evolution

In response to thermally induced subsidence and eustatic sea-level rise, fully marine conditions became established in the Santos Basin by the Albian, and a carbonate dominated succession was deposited on the upper part of the continental slope (Itanhaém Formation; Moreira et al., 2007) (Fig. 5). Post-rift subsidence was at this time focused in the future oceanic basin, resulting in significant tilting of the upper continental slope during the latest Albian. This latter event generated a thin-skinned array of predominantly seaward-dipping normal faults, which segmented the Albian carbonate platform into extensional rafts (Mohriak et al., 1995; Guerra and Underhill, 2012; Quirk et al., 2012). In the study area, a sequence of distal turbidites, submarine fans and mass-transport deposits were deposited after the Albian in response to sediment progradation, moderate salt movement, and local halokinesis (Mohriak et al., 1995; Duarte and Viana, 2007). No extensional rafts are observed, and the post-salt overburden is predominantly shortened (Figs. 2 and 3).

Albian strata are absent on Santos Basin's upper continental slope (e.g. Albian Gap), with some authors interpreting this absence as resulting from Late Cretaceous gravity-driven extension of the post-salt cover (Fig. 1d). Such an interpretation hints at important Late Cretaceous shortening of intra-salt and post-salt strata as a way of accommodating upslope extension (e.g., Mohriak et al., 1995; Modica and Brush, 2004; Quirk et al., 2012). Other authors interpret the Albian Gap as a feature associated with salt expulsion driven by progradation of basin-margin clastic wedges across a pre-existing salt wall (Ge et al., 1997). In this latter case, one should expect no post-Albian shortening of overburden strata in the study area because updip extension on the upper continental slope was not significant after this stage. Nevertheless, the study area shows continued shortening and salt withdrawal into the Cenozoic, particularly in its distal part (Figs. 2 and 3).

3. Data and methods

A three-dimensional (3D) pre-stack depth migrated (PSDM) seismic volume covering 142,800 km^2 of the deep-water region of SE Brazil was interpreted in this paper (Fig. 1a and c). Data processing included Kirchhoff pre-stack depth migration performed on 60 offset volumes (270 m–6170 m), with an input geometry of 18.75 × 18.75 m. A 75 m × 75 m x 50 m velocity model grid was used for the depth migration, and the final pre-processing data was used as migration input. The final 3D seismic volume has a bin size of 18.75 m, a sampling window of 6 m and a sampling depth of 12,000 m. Vertical seismic resolution ranges from 35 m to 45 m at the depth of the pre-salt reservoir, and 15–25 m in post-salt

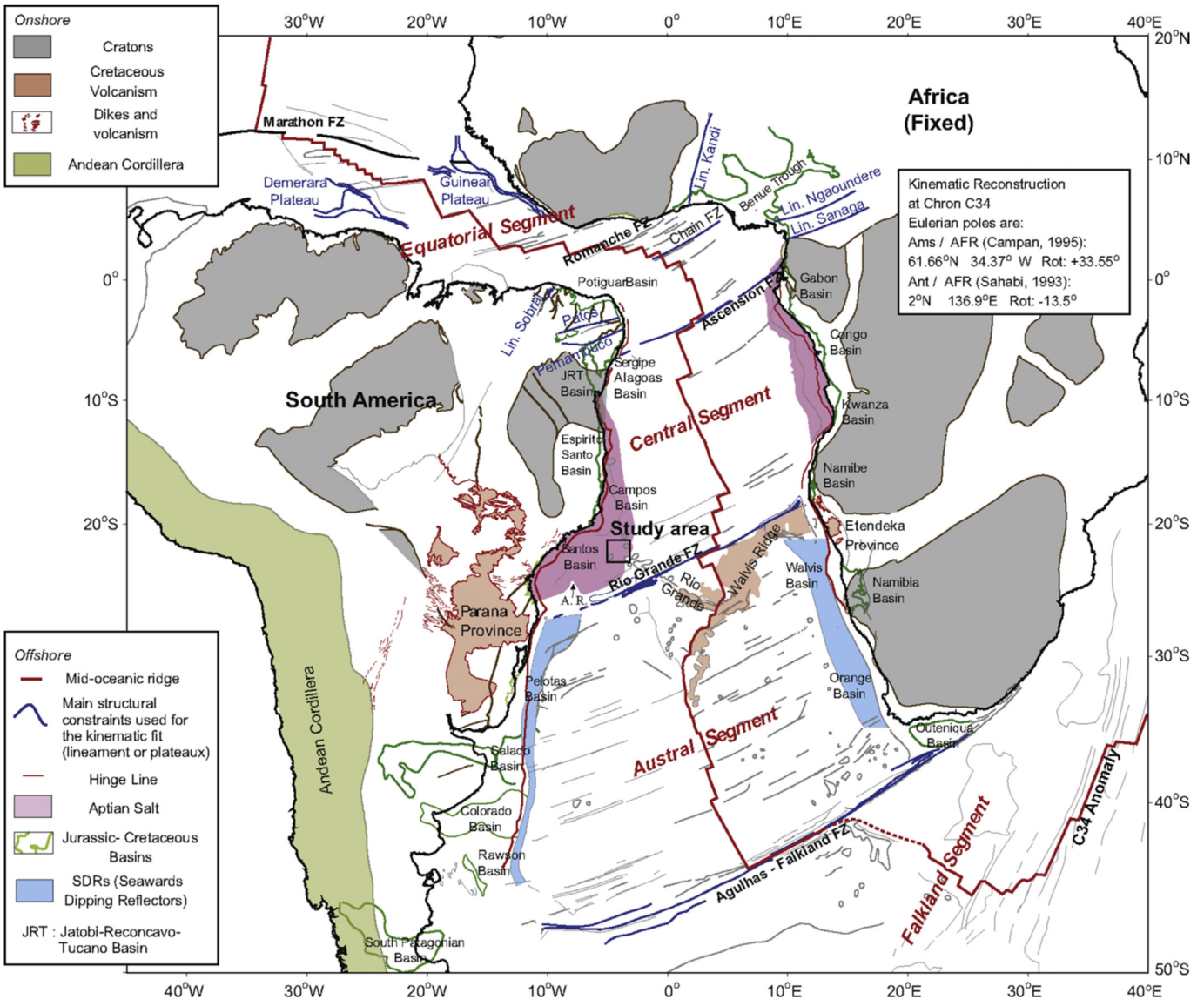

Fig. 4. General tectono-structural map of the South Atlantic Ocean at Chron 34 (84 Ma) as interpreted in Moulin et al. (2010) using Eulerian pole data from Sahabi (1993) and Campan (1995). The figure highlights the location of the study area in relation to main structural and bathymetric features of the South Atlantic Ocean. Fracture zones and seamounts are based on interpretation of satellite-derived gravity 1 mn × 1 mn grid (Sandwell and Smith, pers. comm.). The bathymetric contours near Walvis Ridge are based on the Ifremer detailed bathymetric map (Needham et al., 1986). The large red line represents the accreting oceanic ridge at Chron 34. A.R.-Abimael Ridge; F.Z.-Fracture Zone. (For interpretation of the references to colour in this figure legend, the reader is referred to the web version of this article.)

successions (Figs. 2 and 3).

3.1. Quantification of erosion at pre-salt level

In order to quantify erosion at the top of the pre-salt reservoir we mapped a series of faults crossing the syn-rift and post-rift series, together with deformation features at base salt level, i.e. Horizon S2 (Figs. 1c, 2 and 3 and 5). To quantify pre-salt erosion, we used the structural methods of Roberts and Yelding (1991) developed for the North Sea-Mid Norway rift (Fig. 6). In their interpretation, Roberts and Yelding (1991) propose erosional truncation of syn-rift sequences to be quantifiable through the mapping of reflection truncations across eroded half-grabens. The advantage of this method is that the interpreter can quantify the thickness of data eroded and exhumed on top of footwall blocks when the relationship between fault throw and the presence/absence of 'pre-rotation' sequences is observed on hanging-wall blocks (Fig. 6).

3.2. Quantification of ramp gradients on pre-salt highs

In order to investigate if present-day pre-salt ramps and structural highs correlate positively with the deformation styles of younger strata, we based our analyses on the postulates of Elliott (1976) and Berger and Johnson (1980, 1982), who considered the friction at the basal ramps of thrusts to determine the velocities and stresses in the basal décollement (Fig. 7). Viscous material over the décollement is assumed by the latter authors to adhere to the rigid base, i.e. presenting adhesional drag. The maximum shear stress the base can exert onto the contacting viscous material is the adhesional strength, κ, shown in Fig. 7, which controls the geometry of thrusts above.

The theory of Berger and Johnson (1982) cannot be directly applied to a typical salt-tectonics setting; the more than 2 km-thick evaporites observed in the study area suggest the presence of a weak décollement that will result in the predominance of relatively

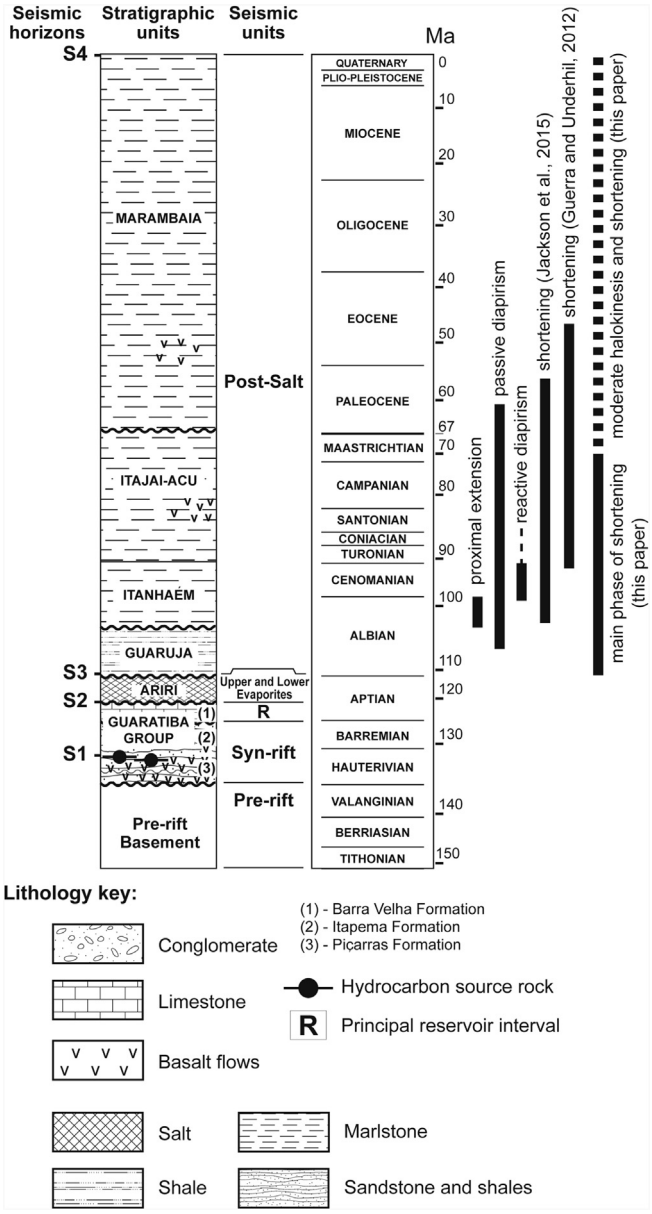

Fig. 5. Summarised lithological column for the study area, deep-water Santos Basin (from Moreira et al., 2007). The Guaratiba Group is divided by the latter authors in three distinct formations: a) Piçarras, b) Itapema; c) Barra Velha. The relative times in which salt tectonics is observed in the study area are shown together with data from Davison et al. (2012), Guerra and Underhill (2012) and Jackson et al. (2015).

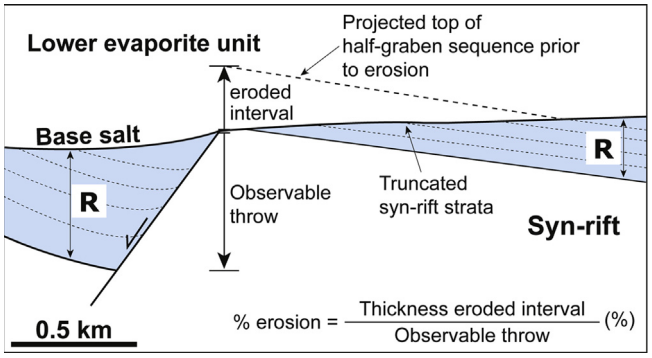

Fig. 6. a) Schematic representation of the structural method of Roberts and Yelding (1991) applied to quantify basin-margin erosion in the North Sea-Mid Norway rift. The figure highlights the relationship between the geometry of rotated reservoir ('R') strata and estimates of erosion over footwall blocks.

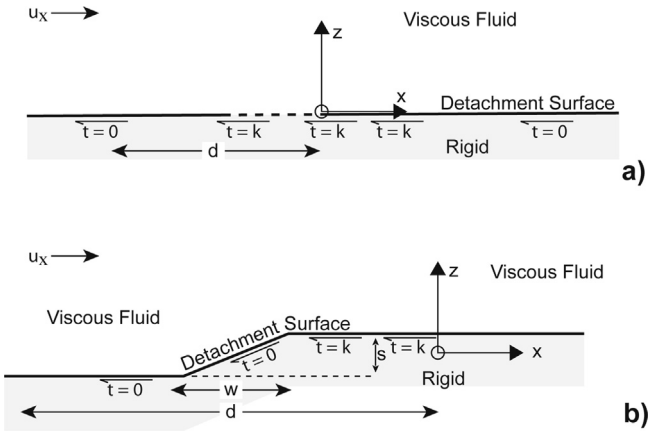

Fig. 7. Shape of detachment surface and distribution of drag as assumed in the theoretical analyses of Berger and Johnson (1982). a) Movement of viscous fluid over a flat detachment surface. Solid heavy line is segment with free slip. Dashed line is segment with drag of magnitude κ. b) Geometry and forces expected in stepped detachment surfaces, which comprise a dipping ramp segment connecting upper and lower flat segments. Heavy line is segment with free slip. Drag on upper flat segment has a magnitude κ. τ - shear force at the décollement.

even synthetic-to-antithetic fault ratios above the salt (Rowan et al., 2000) (Figs. 2 and 3). However, flow velocity and shear drag still increase within salt in the presence of basal ramps (e.g. Butler, 1987; Cotton and Koyi, 2000; Dooley et al., 2007). In order to determine the regions expected to present the larger shear drag value in the Aptian salt, we compiled maps of salt thickness and gradient of ramps below the salt. We then compared the maps obtained with the deformation styles above the salt, and the degree of erosion recorded at base-salt level, i.e. at the top of pre-salt reservoir successions (Figs. 2, 3 and 6). The steeper the ramps, the easier will be to thrust and fold a succession above the salt décollement (Cotton and Koyi, 2000; Rowan et al., 2004).

Ramp gradients were calculated every 250 inlines (4 km) in a N-S direction, i.e. along the pre-salt ramps (Fig. 1c). A total of 441 ramps and flats were measured in this work along 20 different inlines, effectively dividing the interpreted seismic volume in 20 equal blocks, or areas. We calculated ramp gradients as follows:

$$\text{gradient} = \frac{\text{rise}}{\text{run}} \cdot 100 \quad (1)$$

In our calculations, we assumed a low value for shear drag in the flat segments between structural highs H1 to H4 as they comprise zones of low resistance to sliding, with relatively thick salt and flat basal ramps (Figs. 1c and d and 2). In contrast, higher shear drag values are expected on the ramps of structural highs, which also present salt welds at places (Figs. 2 and 3). Ramp gradients were tabled and plotted on Surfer® so they could be compared and contrasted with the regions in which erosion or tectonic truncation of the pre-salt reservoir exceeds 20% of its thickness (Table 1).

4. Seismic-stratigraphy

For the purposes of this paper, five units were mapped in the study area:

a) Pre-rift volcanic/volcanogenic series comprising mostly basalts (Hauterivian-Barremian).

Table 1
Example of values used in the calculation of the ramp gradients shown in Fig. 18. The table shows values taken at random from 441 ramps and flats identified in the study area. Refer to the text and Fig. 7 for an explanation of each parameter used.

Y (km)	X (km)	w (km)	d (km)	w/d *100
0.00	49.88	0.00	90.35	0.0000
3.69	52.92	11.92	90.35	13.1934
7.65	49.88	0.00	91.57	0.0000
7.65	54.14	10.70	91.57	11.6878
12.27	59.13	8.98	93.28	9.6301
17.23	0.00	0.00	85.26	0.0000
58.65	63.48	4.35	80.61	5.3918
58.65	4.99	0.00	80.61	0.0000
82.26	71.86	4.78	80.38	5.9469

b) Syn-rift series, essentially composed of shales and coquina beds of Barremian age.
c) Post-rift series 1, which includes the reservoir interval (Aptian carbonates), marked as 'R' on seismic sections.
d) Evaporite series; massive halite and carnallite at the base (lower evaporite unit), and layered evaporites and carbonates of Aptian age (upper evaporite unit).
e) Post-salt marine sediments; carbonates and shales (Albian to Recent).

The relationship between these seismic sequences and known stratigraphic units is shown in Fig. 5.

4.1. Pre-rift series (upper Valanginian-lower Hauterivian)

The pre-rift series comprises the basal seismic-stratigraphic unit in deep-water Santos Basin (Figs. 5, 8 and 9). The series shows low- to moderate-amplitude internal reflections, and reaches a minimum of 1 km in thickness as it loses amplitude towards the pre-Mesozoic acoustic basement (Fig. 8). The pre-rift series comprises Hauterivian to lower Barremian volcanic extrusive rocks, volcaniclastic sediment and red continental strata deposited below the main syn-rift series (Moreira et al., 2007) (Fig. 5). Basement units underlie the pre-rift series (Fig. 8).

4.2. Syn-rift series (upper Hauterivian-Barremian)

The syn-rift series fills rotated tilt-blocks in deep-water Santos Basin (Figs. 8 and 9). In this paper, we mapped the youngest basalt interval (Horizon S1) to calculate a minimum thickness for the syn-rift series (Figs. 8–10). The series shows marked growth onto basin-bounding faults, and an alternation of high- and low-amplitude reflections. Its thickness reaches >2 km in discrete depocentres to the east of H1 and H3, but is relatively thin (<750 m) over these same structural highs (Figs. 8–10). The syn-rift series is composed of limestones, volcanic sills, volcaniclastic sediment and mudstones, the latter of which include important hydrocarbon source intervals (Moreira et al., 2007) (Figs. 5, 8 and 9).

4.3. Post-rift series 1 (lower Aptian)

The post-rift series 1 contains the main reservoir interval ('R') in deep-water Santos Basin (Fig. 5). This reservoir unit (Barra Velha Formation) is topped by Horizon S2, and comprises transparent to low-amplitude internal reflections showing moderate growth onto main faults, despite the interpreted post-rift position of this unit (Moreira et al., 2007) (Fig. 9). East of structural highs H1 and H3, the geometry of post-rift series 1 (i.e. pre-salt reservoir) suggests it comprises syn-rift strata (see Soares et al., 2012). Thus, thickness variations (and strata growth) are more prominent east of structural highs H1 and H3, where profiles across the main structural highs and adjacent sub-basins reveal important erosion at the top of the series, a character investigated later in this work (Figs. 2, 3, 9 and 10a). Post-rift series 1 has been recognised as comprising microbial carbonates and tufas deposited in hypersaline lakes, some of which are kastified and eroded (Moreira et al., 2007).

4.4. Evaporite series (Aptian)

The Aptian evaporite series shows chaotic to low-amplitude reflections at its base, and continuous, internal reflections towards its top (Figs. 8 and 9). In the study area, the lower evaporite unit (salt) can reach a thickness of more than 2 km, within specific salt walls. The thickness of the upper evaporite unit approaches 0 m over evaporites and salt walls, and is less than 2 km in between developed salt structures (Figs. 2, 3 and 8). Important erosion at the top of the upper evaporite unit is locally observed (Figs. 3, 8 and 9).

Jackson et al. (2014) recognised the presence of basal halite and anhydrite in the series, with higher grade evaporites (and potash salts) such as carnalite and tachyhydrite occurring towards an upper salt member. Some of these potash salts are interbedded with shales (Moreira and Carminatti, 2004, 2007). In the study area, characteristic features in the evaporite series include developed thrust faults and associated anticlines (Figs. 12 and 13). Towards the northeast, thrust anticlines give rise to relatively undeformed salt pillows and salt walls (Figs. 14 and 15). In fact, there is a general tendency for increasing deformation towards the east, particularly over structural highs H3 and H4 (Figs. 12–14).

4.5. Post-salt marine series (late Albian to Holocene)

In this paper we mapped the top of the marine series overlying the Aptian evaporites (Horizon S4, Figs. 10 and 11). The post-salt marine series shows transparent to low-amplitude internal reflections and reaches a thickness in excess of 2 km to the east of structural highs H1 and H3 (Figs. 11–13). The series denotes moderate halokinesis and is bounded at its base by a prominent 'top salt' unconformity (Figs. 9 and 11). Prograding reflections are also visible to the northeast of H2. The post-salt marine series comprises deep-marine strata such as hemipelagites and pelagic mudstones (Moreira and Carminatti, 2004, 2007).

5. Thick-vs. thin-skinned structures

5.1. Pre-salt horsts and grabens

In the study area, pre-salt units are deposited in grabens and half-grabens underneath a thick lower evaporite (salt) succession that reaches >2 km in thickness (Figs. 8, 9 and 10a). As a result of rifting, distinct fault families are observed below the Aptian salt, from which the most developed family is NE-trending (Figs. 1c and 10). Normal faults bound main structural highs at pre-salt level, and comprise a series of linked segments with a length exceeding 40 km (Figs. 8 and 9). Tilt-blocks, as well as faults bordering them, were generated during the pre-Aptian continental rifting that eventually led to continental breakup between SE Brazil and West Africa (Moulin et al., 2010).

The study area comprises four pre-salt structural highs, H1 to H4, with average ramp crests at ~5000 m depth for H2, H3 and H4, and ~5500 m depth for H1 (Figs. 10a, 11 and 12). These four structural highs comprise distinct pre-salt ramps. Importantly, east of H1 and H3 occur highly-rotated crustal blocks that denote important crustal stretching (Figs. 2 and 13). Crustal extension in this region caused significant rotation of tilt-blocks over a thinned lithosphere (Fig. 2). In contrast, to the west of H1 and H3 pre-Aptian

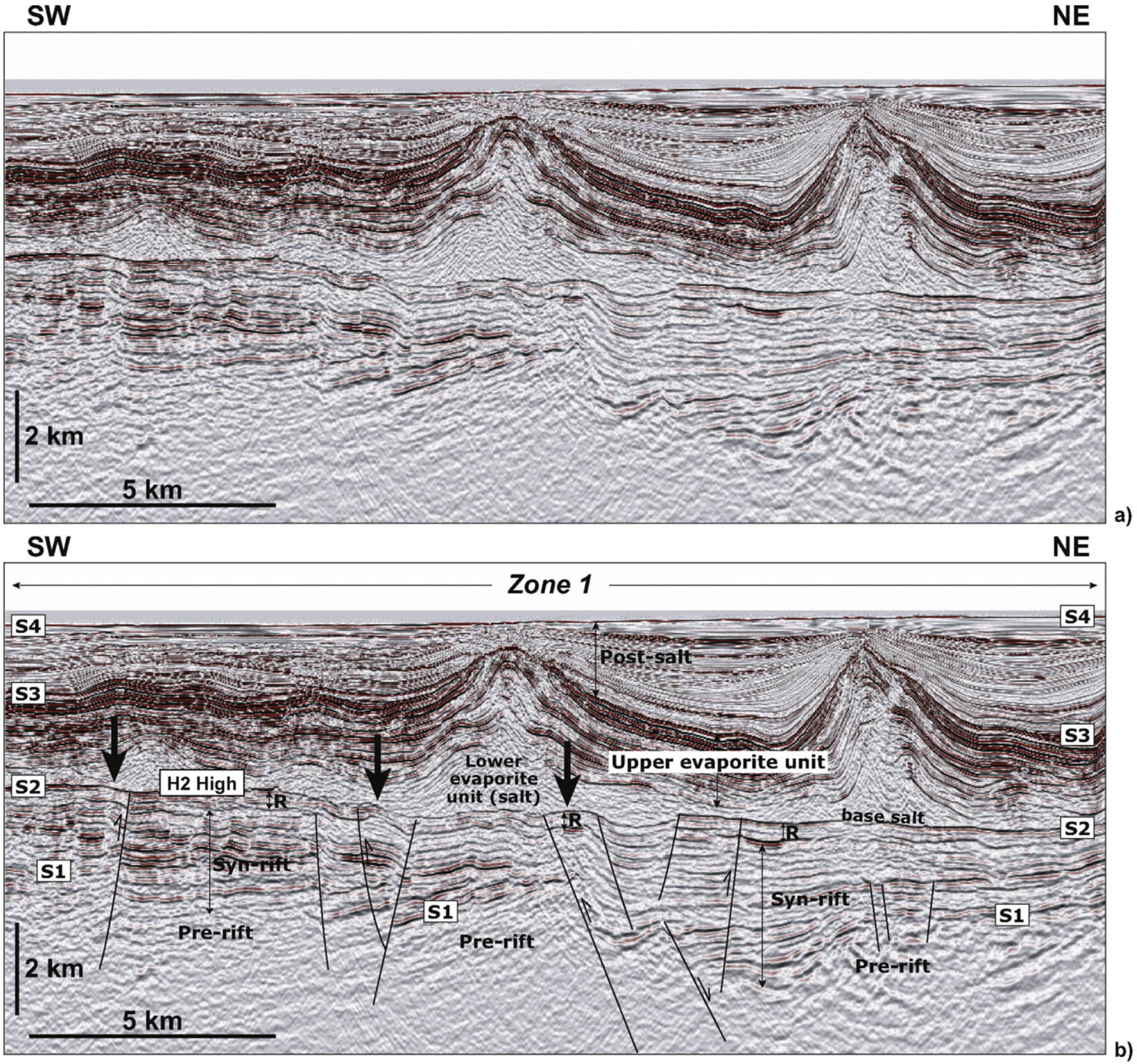

Fig. 8. Composite PSDM seismic lines from the region north of H2. a) Uninterpreted profile. b) Interpreted profile highlighting the presence of small-scale pop-up structures at reservoir level, probably associated with the reactivation of a normal fault in depth. See Fig. 1c for location of the seismic line. Thick arrows highlight the location of reactivated normal faults on the interpreted seismic section.

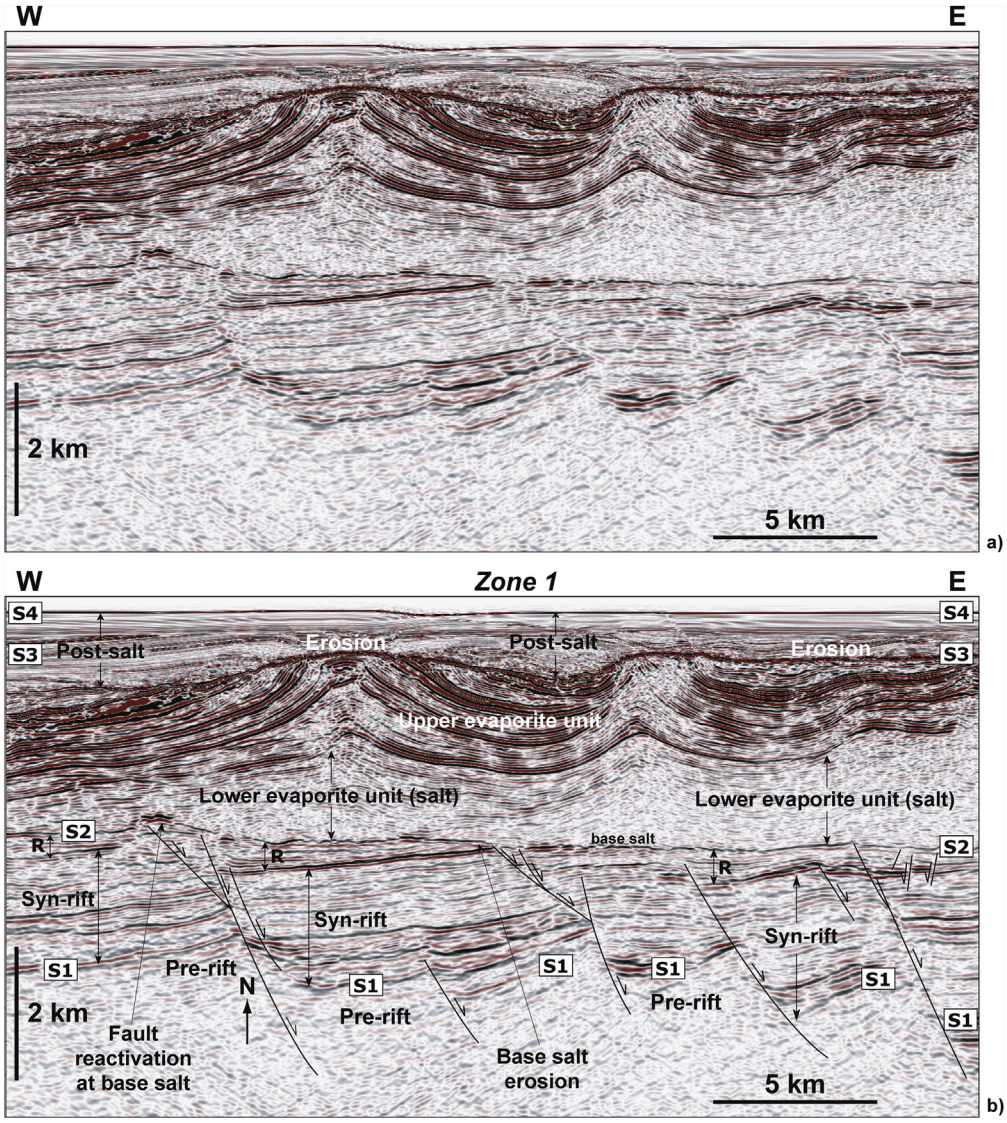

Fig. 9. a) Seismic profile from the region north of the H2 High. The profile shows developed minibasins developed in the Late Cretaceous and Early Cenozoic. Note the presence of local inversion in reservoir units (R). The figure also highlights the widespread erosional truncation observed at top reservoir level, with tilted blocks virtually flattened at base salt.

crustal extension was accommodated by normal faults showing relatively moderate displacements (Fig. 11). For instance, Figs. 11 and 12 show NE-trending faults with relatively small displacements, but forming a series of structural steps until the summit of structural highs are reached. Figs. 2, 3 and 13, in contrast, show examples of NE- and NW-trending faults that delimit prominent structural highs, generating eroded footwall blocks at several locations.

Tectonic inversion at pre-salt level is recorded in different areas of the interpreted seismic volume, but it is notably more intense in the region north of H2 and around H1 (Figs. 15 and 16). In these areas, the majority of inversion structures comprise reactivated syn-rift normal faults, either forming strike-slip structures or transpressive and transtensional features (Figs. 8 and 9). Fault reactivation is observed at different levels in the pre-salt successions, i.e. there is no clear concentration of inversion in a specific horizon, or unit. Examples of this non-selective reactivation are shown in Figs. 8 and 9, with syn-rift normal faults deforming reservoir and syn-rift units after their deposition.

Inversion structures at pre-salt level chiefly occur where N- and NE-trending faults coalesce. In this region, normal faults formed during the syn-rift stage were reactivated as low and high-gradient reverse faults and pop-up anticlines (Figs. 8 and 9). We note in Fig. 8 the presence of inversion structures towards the southwest, whereas normal faults intersect syn-rift units, the main reservoir, and the base salt horizon in other parts of the seismic profile. This character indicates that tectonic reactivation occurred after the deposition of the reservoir unit. Significant erosion is observed at top reservoir level, particularly above the area where inversion is recorded in Fig. 9. In other regions, the reactivation of syn-rift structures is relatively mild, with extension likely predominating prior to, and also soon after, the deposition of Aptian salt (Figs. 15 and 16).

5.2. Post-salt gravitational gliding, folding and thrusting

Seismic data reveal the presence of three different zones in terms of observed salt deformation styles (Figs. 14 and 17). Zone 1 comprises wide minibasins denoting limited thrusting of salt anticlines. Asymmetric salt anticlines verge moderately to the

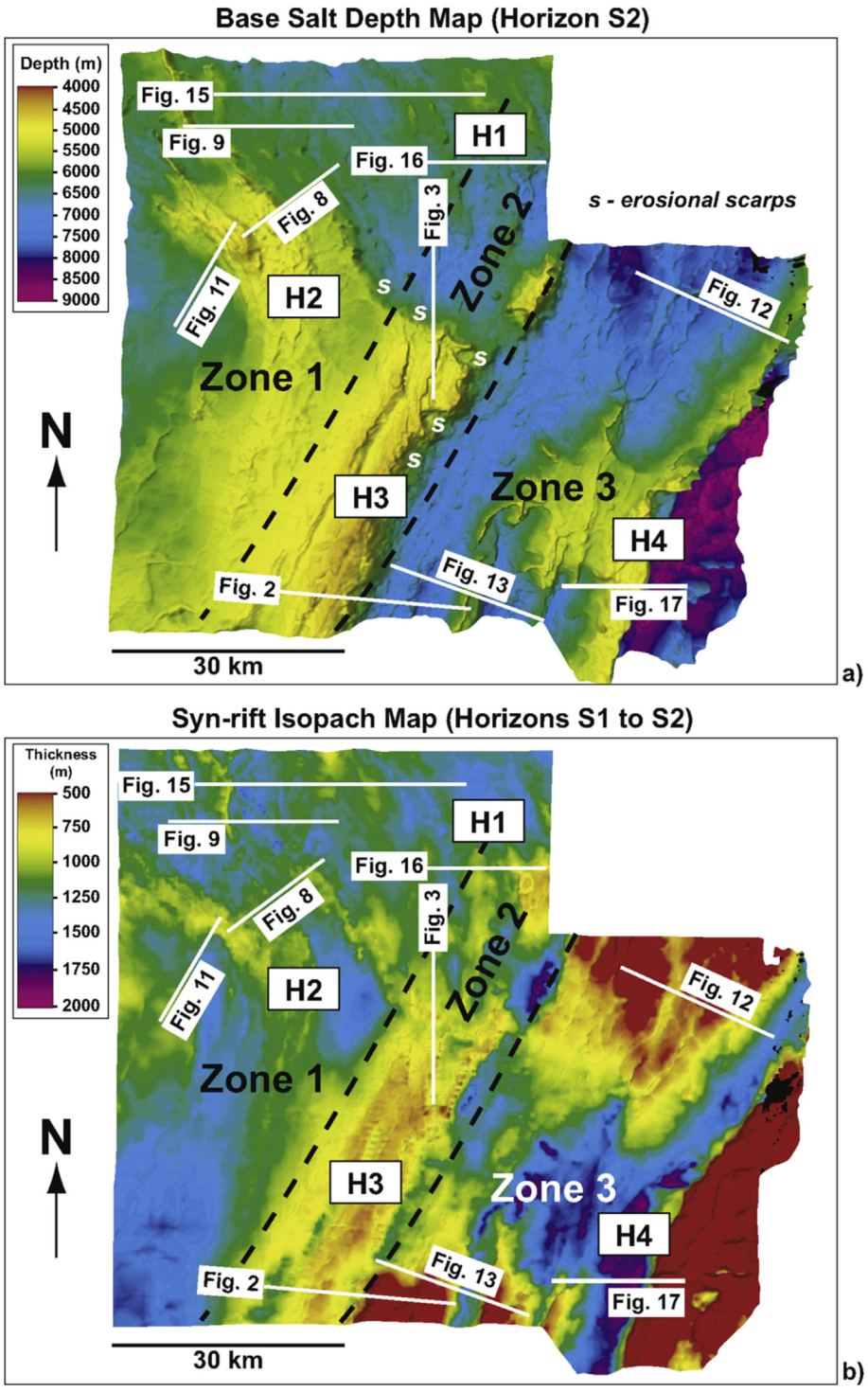

Fig. 10. a) Depth map of the base salt surface (Horizon S2) highlighting the relative position of the three deformation zones in relation to the underlying the pre-salt structure. b) Isopach map of the upper syn-rift sequence i.e., interval between the top of the Piçarra Formation (Horizon S1) and the base of the Ariri Formation (Horizon S2). In the figure are shown the location of the principal syn-rift depocentres post-dating the emplacement of the youngest basalt interval in the study area.

southeast, but thrust faults are not observed within the Aptian evaporites (Figs. 11 and 15). Significantly, the thickness of the Aptian salt is lower in Zone 1 when compared to Zones 2 and 3 (Figs. 11, 13 and 14).

Zone 2 comprises a region of tight folding in the upper evaporites and overlying strata, with local duplex structures and eroded salt anticlines (Figs. 2 and 3). Southeast-verging thrusts and salt walls form a series of tight ridges aligned NE-NNE in Zone 2 (Figs. 2 and 3). Above H1 and H3, the significant erosion observed on top of the upper evaporite unit suggests these two structural highs were uplifted during the late Aptian-Late Cretaceous, and controlled salt deformation above. Such a character is further highlighted by the presence of thin or absent Cretaceous units in most part of Zone 2 (Figs. 2 and 3). Thrusting is moderate over H3 (Fig. 2), but fully

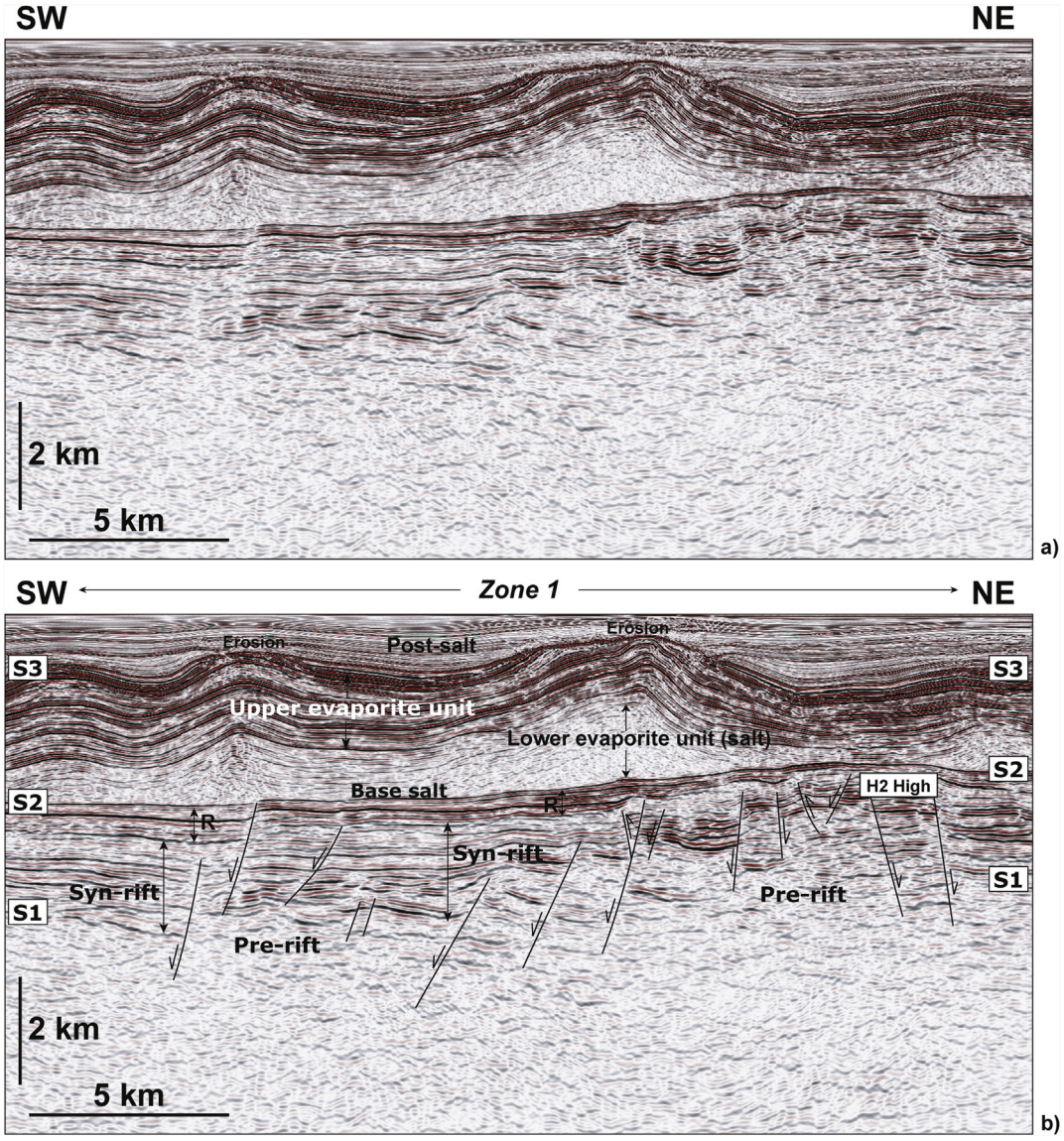

Fig. 11. a) PSDM seismic profile from the region north of H2. See Figs. 1c and 10 for its relative location. The figure depicts a series of N-trending faults that intersect the NW-trending family. A significant thickening of strata towards N-trending faults is a characteristic of this same family in the entire 3D volume. Erosion is recorded only locally, and very moderately (if at all) above H2.

developed piggy-back thrusts occur between H1 and H3.

Zone 3 reveals a complex evolution, highlighted by the salt minibasins and thrusted salt anticlines observed, some of which are active at present (Fig. 12a and b). Thrusts and salt withdrawal basins are more developed in Zone 3 that in the remainder of the study area. Thrusts are SE-verging as in Zone 2, with synthetic-to-antithetic fault ratios between 6/1 to 8/1 (Figs. 13 and 17).

To the east of H1 and H3, the bulk of salt deformation occurred from the Aptian to the end of the Cretaceous (Figs. 13, 14b and 17). However, moderate halokinesis and folding continued until the Late Cenozoic (Figs. 13, 14b and 17). In general, salt movement is more intense east of H3 and between H1 and H2, where developed salt withdrawal basins were formed (Figs. 15 and 16). In parallel, the distal margin records important halokinesis after the Cretaceous. Fig. 17, for instance, shows an E-W profile across structural high H4, over which significant halokinesis is observed. Growth of strata in individual minibasins is observed relatively early within the upper evaporite unit, whereas Albian to Paleogene strata show the largest thickness variations (Fig. 17).

6. Salt deformation above pre-salt structures and associated top reservoir erosion

Fig. 9 denotes significant erosion at the top of reservoir strata on the northern flank of H2 to illustrate the relationship between salt structure and pre-salt erosion. The reservoir ('R') is intersected here by a series of normal faults whose movement precedes the deposition of this same unit. A key observation is that a substantial part of strata topping the syn-rift succession was eroded prior to salt deposition, most likely due to sub-aerial exposure over uplifted structural highs (Figs. 3, 8 and 9). However the area shown in Fig. 9 is, at present, distant 20 km to the north of the H2 structural high; erosion is observed throughout the northern flank of H2 towards an extensional basin formed between H1 and H2 (Figs. 9, 10a and 15). This shows an important discrepancy between top reservoir erosion, pre-salt topography, and thrust geometry, suggesting that the Early Aptian pre-salt topography was different to that presently observed in the study area.

Contrasting with large parts of the lower continental slope of SE

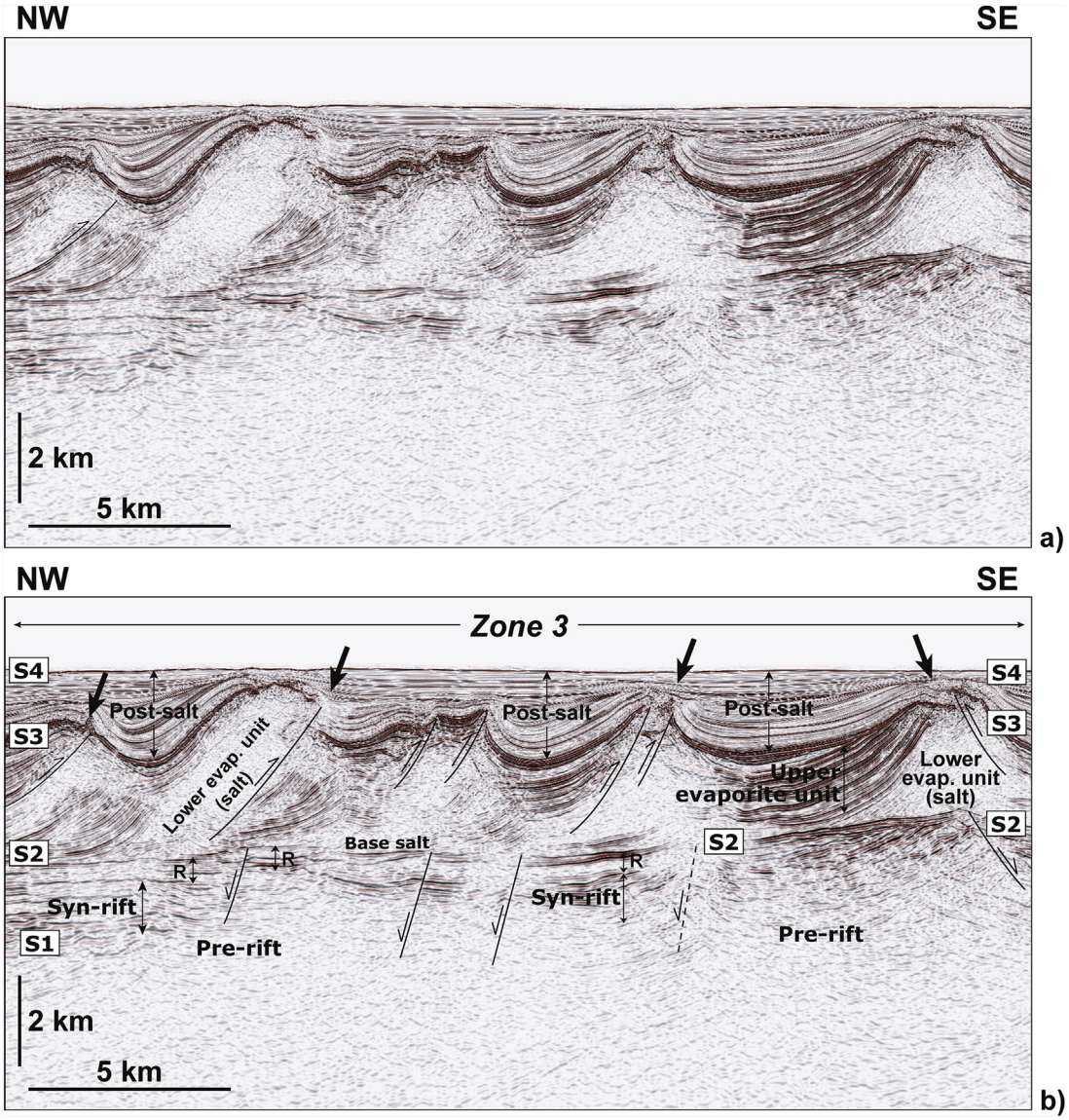

Fig. 12. PSDM seismic profile across Zone 3. See Figs. 1c and 10 for location. The profile shows a series of developed thrusts over salt walls in the region north of H4. Arrows highlight the location of the largest thrusts.

Brazil, where salt canopies and near-seafloor extrusion of evaporites occur (Fiduk et al., 2004), the study area shows a simpler geometry, with salt walls, and relatively small diapirs penetrating the Cenozoic overburden. The most striking features are the tight folding and thrusting experienced by the salt over major rift-related tilt blocks. While Dooley et al. (2015) and Jackson et al. (2015) favour density inversion within autochthonous salt (i.e., lower evaporite unit) to justify diapiric rise through simple fold amplification of internal salt stratigraphy, there is evidence in the study area for significant thrusting and gliding of salt over pre-salt reservoir units (Figs. 3 and 11 to 14). The intra-salt structures observed accompany regional shortening of overburden units and suggest a style of intra-salt deformation distinct from Dooley et al. (2015) and Jackson et al. (2015).

In order to justify the post-salt geometry interpreted on seismic data, we considered a quick translation of salt during the Aptian-Late Cretaceous in our calculations. Our postulate was based on the marked post-salt deformation observed in and after the Aptian in the study area (Figs. 13, 16 and 17). Fig. 18 shows the calculated ramp gradients, which imposed basal barrier to a moving salt layer of a certain viscosity and velocity. In this same figure, we compare the distribution of ramp gradients with the regions where erosion of more than 20% of the pre-salt units is observed on seismic data (e.g. seismic profile in Fig. 9).

Cotton and Koyi (2000) demonstrated that tight asymmetric folds and thrusts are formed in regions of higher shear drag in salt, with broad symmetrical folds occurring when drag approaches zero (0). However, tight folds, thrust ramps and imbricate reverse faults are formed between structural highs H1 and H3, in a sub-basin separating these two highs, and not over the larger H3 high - which shows relatively small ramp gradients in its northern part (Fig. 18). At present the largest ramp gradients are recorded over H2 (Zone 1) and in the northern part of H1 (Zone 2) (Fig. 18). Thrusting is ubiquitous above H1, but is virtually absent above H2 where evidence of erosion is also sparse at base salt level (Figs. 11 and 16). Furthermore, complex folding is observed over structural high H4 (Zone 3), with thrusts and duplexes not necessarily formed over pre-salt ramps (Fig. 17). Here, ramp gradients approach those of H2

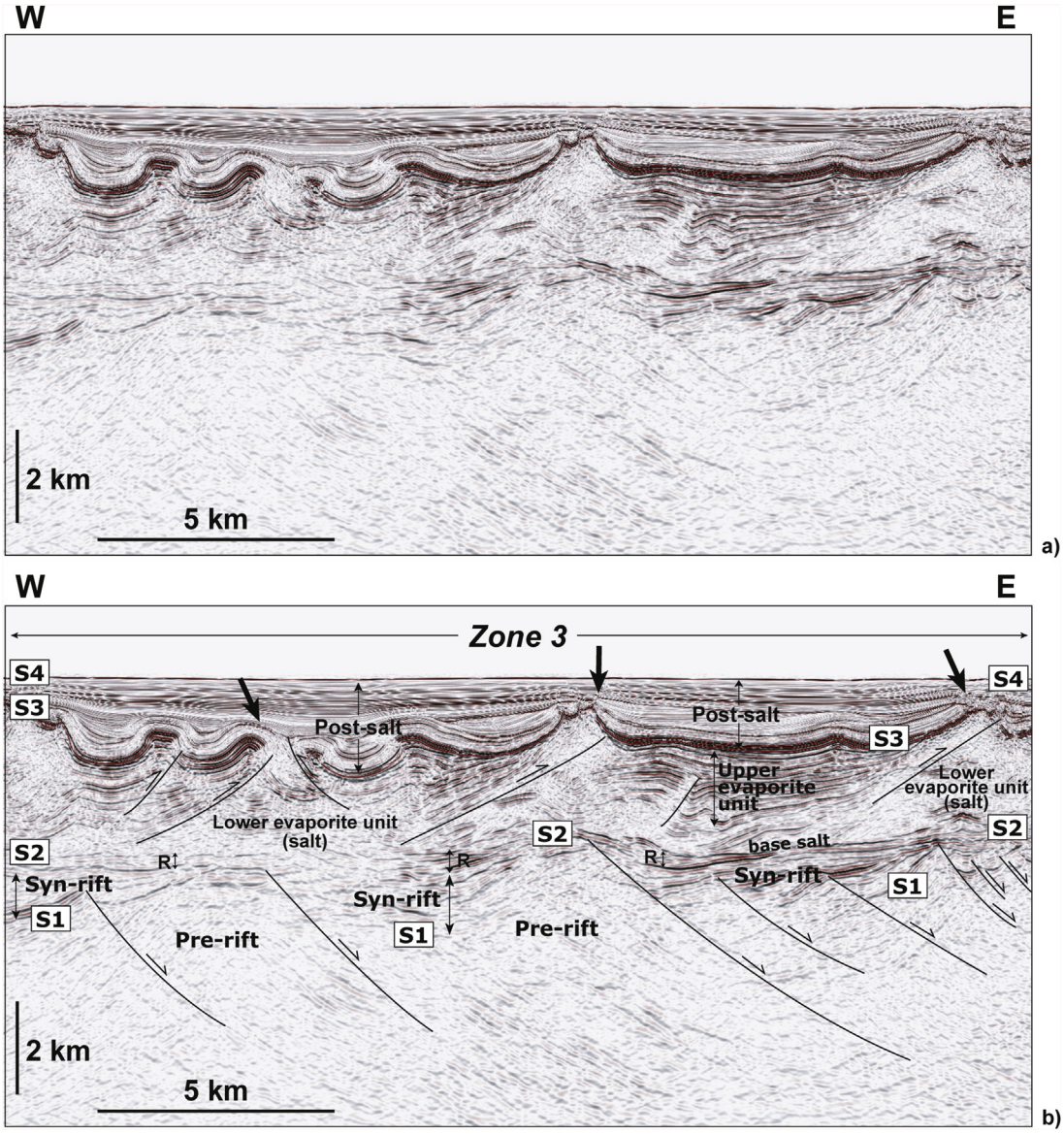

Fig. 13. PSDM composite section across thrust ramps in Zone 3. See Figs. 1c and 10 for location of the seismic line. The profile depicts a series of harmonic folds in Albian-Upper Cretaceous strata. By the end of the Albian folding essentially ceased in this region, leading to the generation of broader salt withdrawal basins on top of the harmonic folds. Areas with folded and uplifted Upper Cretaceous-Cenozoic overburden are highlighted by the thick arrows.

(Fig. 18).

7. Discussion

7.1. Discrepancy between calculated drag, overburden shortening and pre-salt erosion

A key question that arises from our results is why the reservoir unit is truncated by more than 20% away from structural highs H1 to H4? Is this a result of pre-salt erosion over structural highs that subsided after the early Aptian, or the product of significant erosion at the base of the Aptian salt? Furthermore, why are some thrusts developed precisely where pre-salt ramp gradients are low at present? Based on the presence of rotated and truncated pre-salt strata through a vast area between H1 and H2, three distinct explanations can be considered – all reflecting significant tectonic reactivation of pre-salt structures.

A first way of explaining the discrepancy between the ramp gradients, overburden shortening and pre-salt erosion is by assuming important thickness and lithological variations in the salt layer. Aptian salt is thicker in Zone 3, where folding is more complex (Figs. 14a and 17). This character may reflect higher ductility for salt deposited in Zone 3, either due to being thicker, or due to post-depositional 'softening'. In fact, sudden increases in water content and heat flow through salt basins are known to cause significant variations in salt viscosity (Weijermars et al., 1993); the relative thin, and significantly extended continental crust observed in Zone 3 suggests heat flow through the salt unit to have been significant during and immediately after rifting (Fig. 17). The thickness of salt is also larger in Zone 3, a factor increasing its mobility and the ductility of a putative basal décollement (e.g. Gemmer et al., 2005). However, the inverse relationship observed between post-salt sediment thickness (i.e., loading) and the degree of deformation observed in Zone 3 suggests an alternative mechanism for salt deformation in the distal margin of SE Brazil.

A second explanation assumes erosion of the pre-salt reservoir

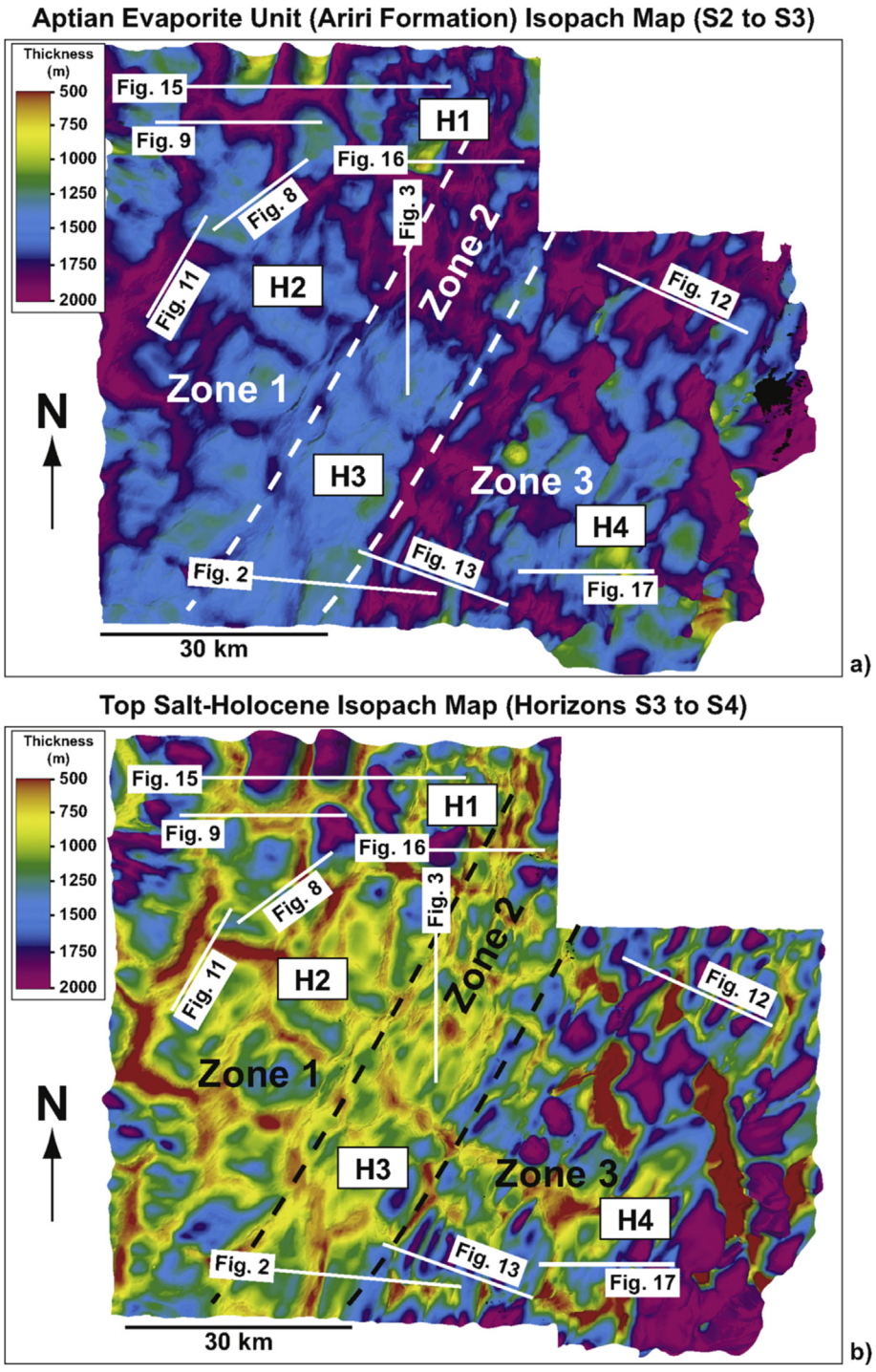

Fig. 14. a) Isopach map of the Aptian evaporite unit (Ariri Formation) in the study area. A NE-SW ridge with thin strata is observed connecting H2 and H3. Note the strike orientation of Zones 1 to 3 in relation to the latter NE-trending H3 high. Zones 2 and 3 are characterised by large thrust faults crossing the upper evaporite unit and overlying strata. b) Isopach map of the Top Salt-Holocene highlighting the three main zones considered in this work. Note the development of multiple salt withdrawal basins in Zones 1 and 3 at this time. Many of these salt withdrawal basins are accompanied by thrust faults and significant deformation of the upper evaporite layer, as shown in Figs. 12 and 13.

due to sub-aerial exposure prior to the deposition of Aptian salt. In this case, the degree of erosion observed below the salt should correlate with present-day pre-salt structures, with large eroded areas being preferentially located over structural highs, and little erosion being observed over depressed grabens/half-grabens (e.g. Figs. 9 and 15). If one assumes no significant vertical movements in the pre-salt succession after the Aptian, the truncation of more than 20% of reservoir strata should reflect sub-aerial conditions after the deposition of the reservoir interval (R), with significantly deeper conditions occurring in sub-basins bounded by main syn-rift faults. This interpretation fits well with the smaller thickness of syn-rift and reservoir (R) strata observed over the main structural highs, but does not correlate with the existence of vast areas of erosion east of H1 and between H1 and H3 (Figs. 9, 15 and 18). The presence of vast areas of top-reservoir erosion off the present-day (pre-salt) structure implies: a) important vertical movements affecting the

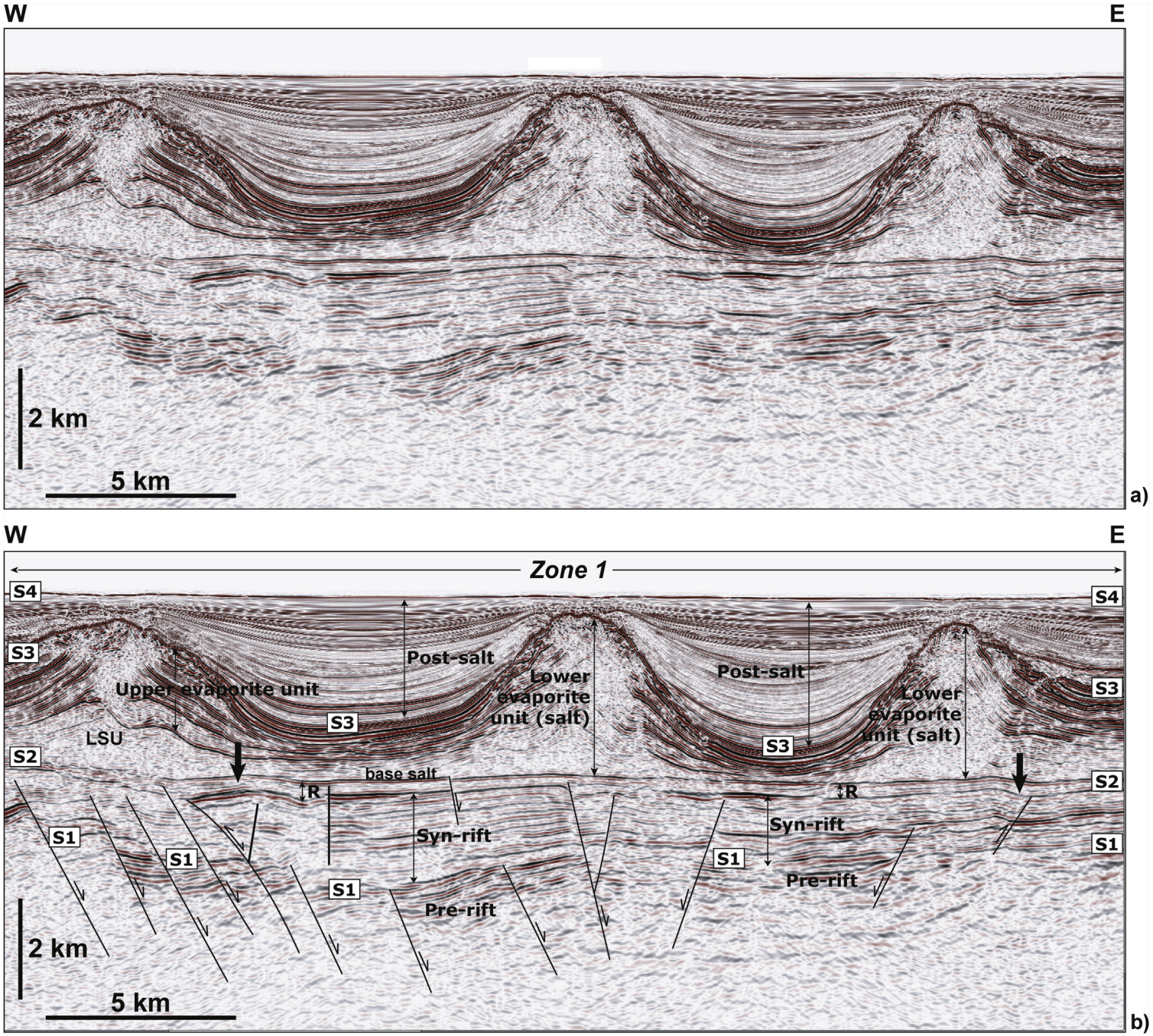

Fig. 15. Composite PSDM seismic lines from Zone 1, located to the east of structural high H1. a) Uninterpreted profile. b) Interpreted profile highlighting the development of large salt withdrawal basins in this part of the study area, and the relatively flat base salt horizon.

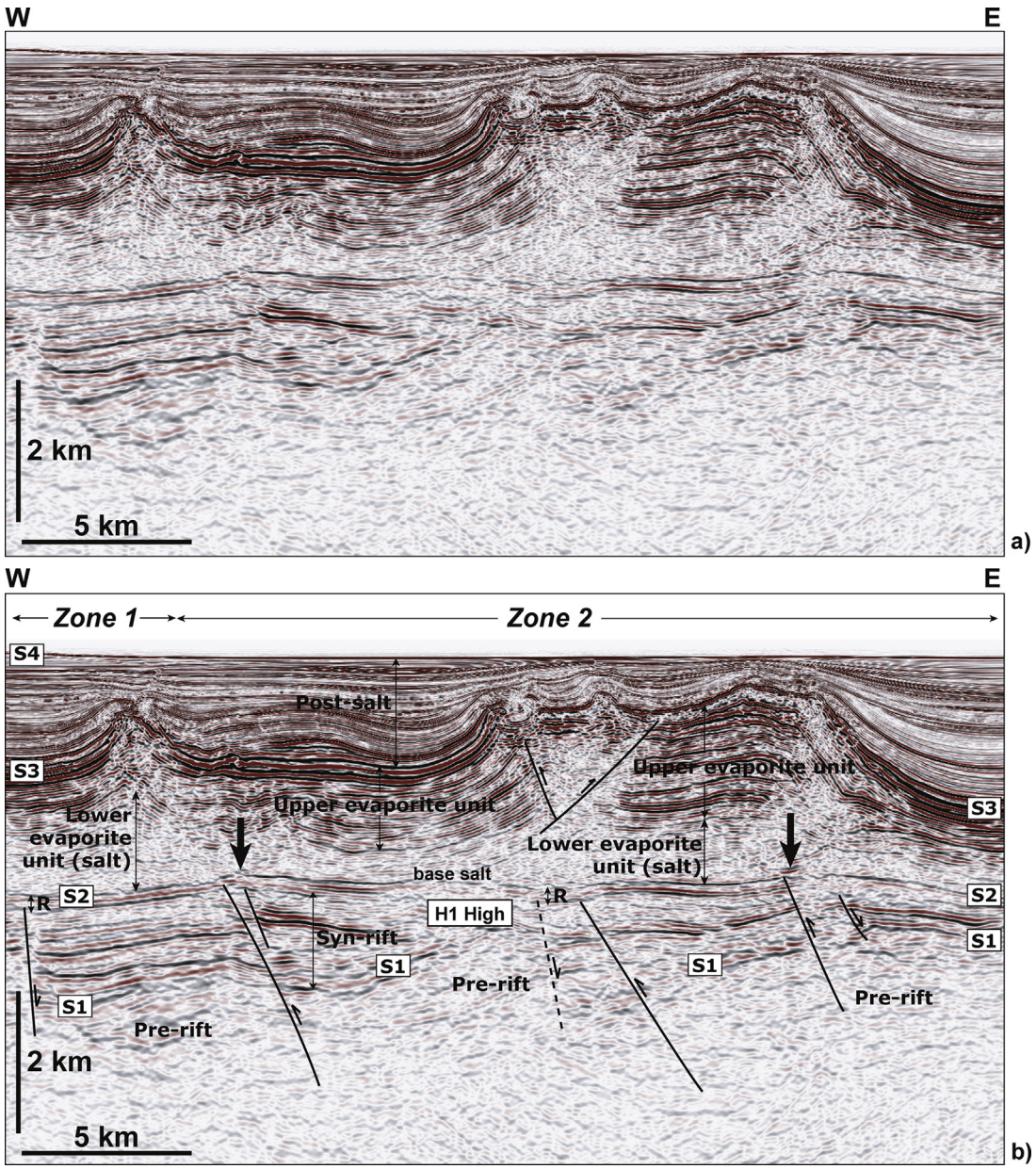

Fig. 16. Composite PSDM seismic lines from the region adjacent to the H1 structural high (Zone 2). a) Uninterpreted profile. b) Interpreted profile highlighting the degree (and styles) of fault reactivation at pre-salt level, and corresponding salt deformation styles in Zone 2.

pre-salt succession since the Late Aptian, and b) that any discrepancies between intra-salt thrusting and pre-salt structure relate to vertical movements of the pre-salt succession after the Aptian.

A third explanation arises if a new concept is considered; that of tectonic truncation at base-salt level in parts of the study area, particularly where the top reservoir horizon (S2) is flat and pre-salt units have been markedly eroded at their top (Figs. 3 and 9). This is a novel concept, but one we suggest after considering Weijermars et al. (2014) recognition of important shear stresses at the base of moving salt units (Fig. 19). Physical models in Dooley et al. (2007) further stress the effect of structures at base-salt, with pinch-outs (where the thickness of salt is reduced) showing an abrupt increase in basal friction and thrust asymmetric vergence. Enhanced basal friction while salt was moved downslope may have accentuated (and promoted) tectonic truncation at the top of the reservoir unit, contributing for the relatively 'flat' geometry it now presents on seismic data (Figs. 11–13 and 15 to 17).

Either resulting from sub-aerial erosion or tectonic truncation due to the gliding of >2 km of salt over syn-rift topography (or a combination of the two processes), the observed discrepancy between the measured present-day ramp gradients, thrusting, and erosion at the base of salt is unambiguous, and hints at significant reactivation of pre-salt structures after the Aptian. We fully support this latter interpretation, and confirm that the boundaries between Zones 1 to 3 coincide with major shifts in the magnitude of crustal stretching at pre-salt level (Figs. 2 and 3). The more proximal Zone 1 records moderate syn-rift extension, but shows no thrusting. Over H3 (Zone 2) there is pronounced thrusting and base-salt erosion, and post-rift fault reactivation was important. In the distal part of the study area, where marked crustal stretching led to the formation of highly rotated tilt-blocks, likely reactivated after rifting, Aptian evaporites are ~30% thicker than to the west, thrusting is

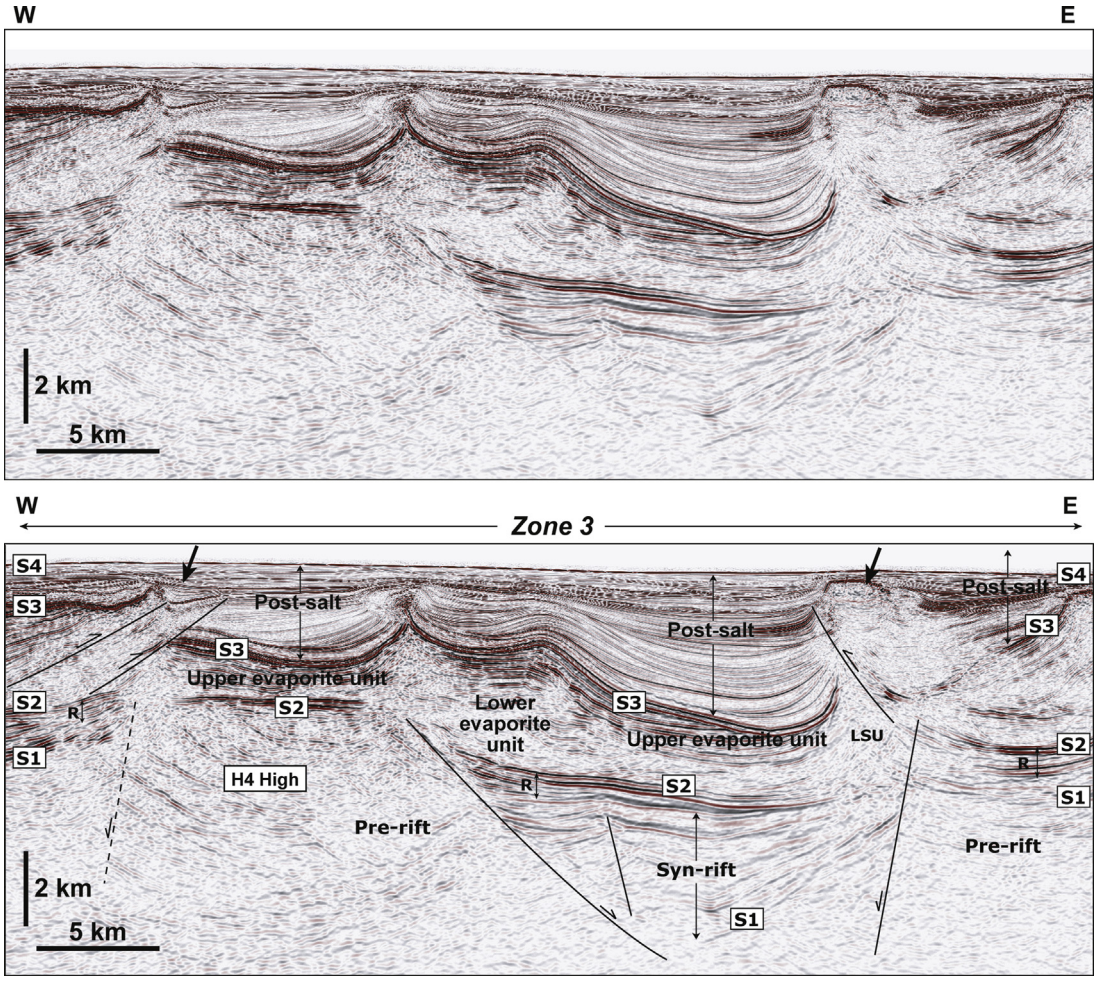

Fig. 17. Composite PSDM seismic lines from the region adjacent to the H4 high (Zone 3). a) Uninterpreted profile. b) Interpreted profile highlighting the geometry of thrusts in the distal part of the study area. Arrows highlight Cenozoic halokinesis and thrusting in the interpreted seismic section.

widespread and halokinesis was relatively prolonged in time (Fig. 17). Reactivated tilt-blocks presenting high ramp gradients at present, but over which erosion and thrusting are irrelevant, can thus be identified as tectonically reactivated areas, i.e. pre-salt highs uplifted after most part of the salt was translated and folded. In such a setting, the downslope translation of >2 km of evaporites over the reservoir unit (R), from the Aptian to the present day, justifies the apparent flattening of the top reservoir (surface S2) observed on seismic data (Figs. 12, 15 and 16).

7.2. Ridge push as an added tectonic driver for salt deformation

When dealing with salt intervals with significant lithological heterogeneity, one key issue concerns the effect of these same heterogeneities in time. For how long can salt deform before generating developed welds is a crucial aspect to investigate when assessing pre-salt erosion, the timings of formation of salt welds in the study area and, indirectly, fluid migration (e.g. Jackson et al., 2014). Resistance in the salt is often considered very low when compared with the basal décollements of convergent margins, and salt layer weakness allows the overburden to be moved downslope for great distances, generating a broad fold-and-thrust belt. The effect of prolonged movement on post- and intra-salt faults, seal competence and fluid transmissibility across salt units is an important aspect controlling the petroleum potential of deep-water basins in SE Brazil, and of other salt-rich continental margins (Mello et al., 1995).

Figs. 12 and 13 show a series of thrusts within the salt that have, in places, propagated into the post-Aptian succession, whilst in other parts of the study area do not reveal thrust propagation above the top salt horizon. In essence, folds in Zone 1 were formed sometime between the end of the Aptian (top salt unit) and the end of the Cretaceous, as the Albian unit is draped by nearly undeformed post-Cretaceous strata (Fig. 16). From the Early Cenozoic onwards, large-scale salt withdrawal basins were developed in the region, but denote relatively moderate movement(s) of the underlying salt (Fig. 13b).

To the east of structural highs H1 and H3 (Zone 3), where post-rift subsidence and post-salt overburden thickness are more pronounced, horizontal shortening in the upper salt layer is so pronounced that piggy-back thrust nappes are locally observed (Figs. 13 and 17). Intra-salt deformation in Zone 3 is, therefore, more intense where post-salt overburden is thicker. As larger thickness values in strata above thrust-and-fold belts have been considered as hindering factor to thrusting and folding (Dahlen, 1990), we suggest that this character relates to enhanced folding resulting from gravitational collapse from the northwest, and horizontal shortening imposed from the east, with H1 and H3 forming local ramps to thick, horizontally shortened evaporite units. The most plausible triggers of horizontal shortening are thus a combination of gravitational gliding (or spreading) and ocean-ridge push on a distal continental margin still close enough to a newly-formed

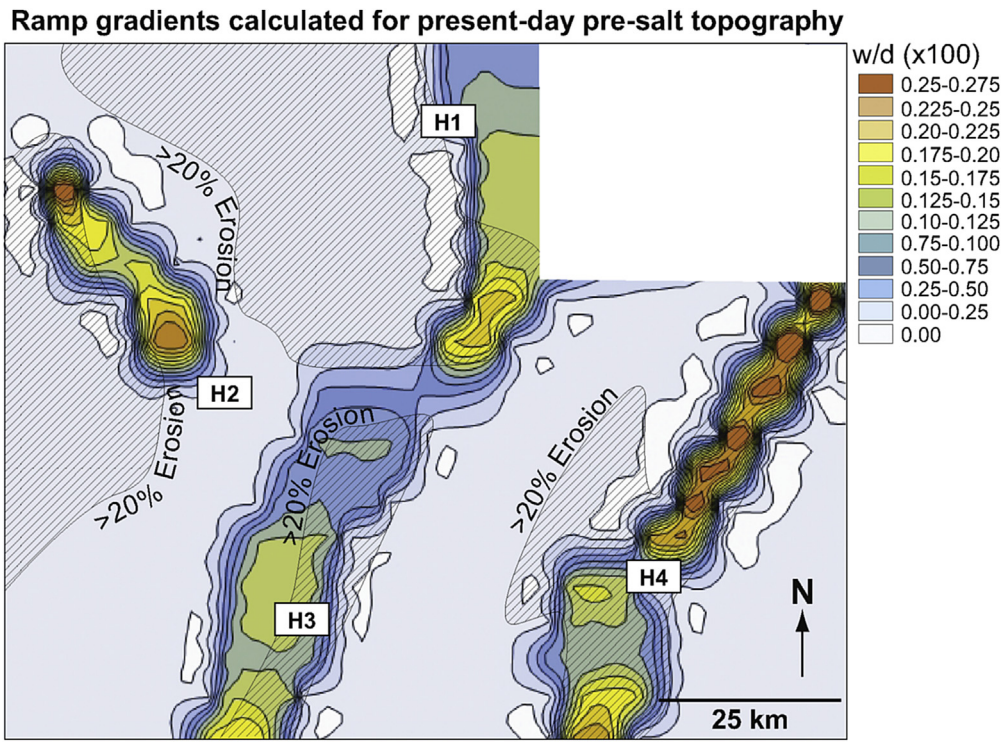

Fig. 18. Map of the study area showing present-day ramp gradients in the study area, and the relative location of regions showing >20% erosion in pre-salt strata. Note the incomplete correlation between the two properties, with the regions between H1 and H2, and south of H2, denoting important erosion.

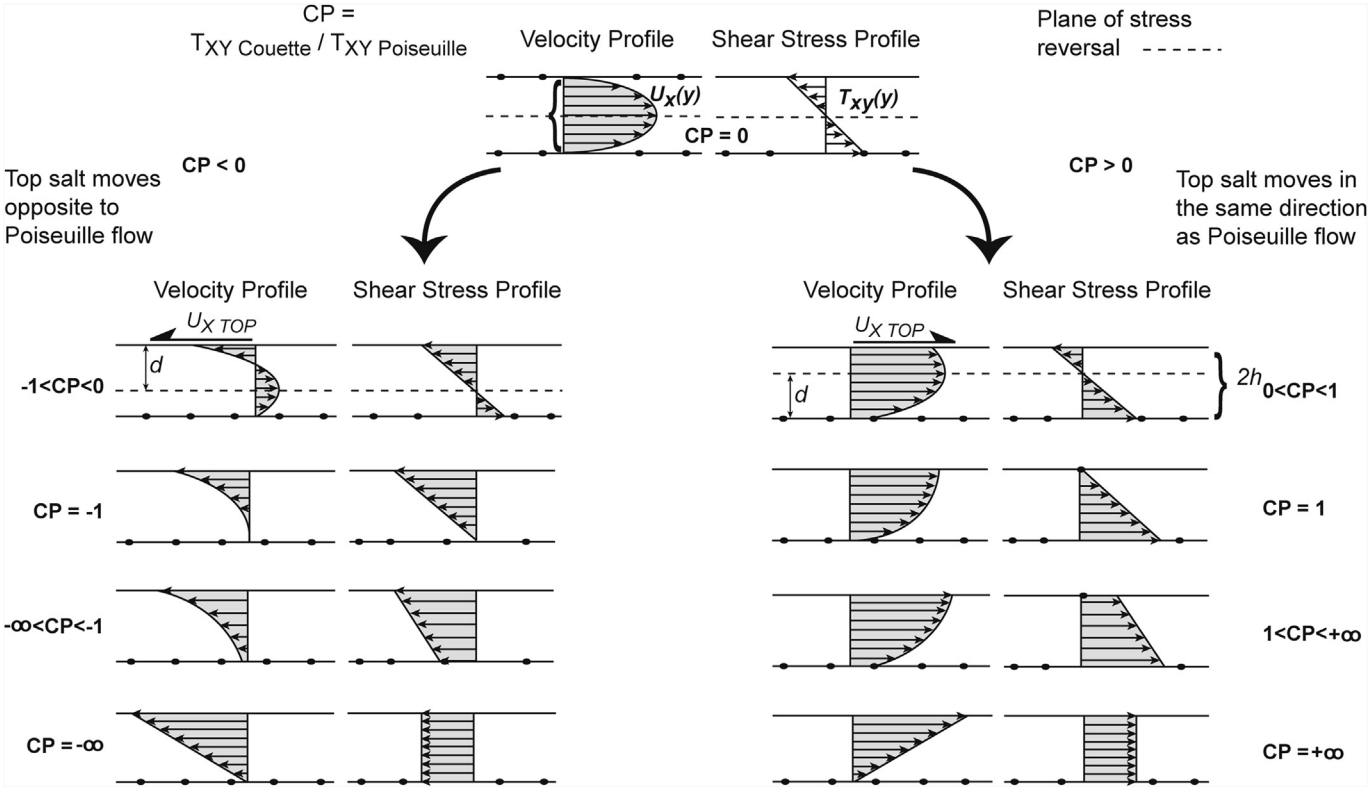

Fig. 19. Summary of full Couette–Poiseuille (CP) number ranges based on the analysis in Weijermars et al. (2014). On the left-hand side are flow profiles and shear-stress gradients for negative CP numbers. On the right-hand side are shown flow profiles and shear-stress gradients for positive CP numbers. Note the direct relationship between the velocity gradients and the shear stresses observed, i.e. the larger the velocity gradients the larger the stress imposed on a volume of salt.

mid-ocean ridge. We suggest that distal parts of the Santos Basin were affected by E-W to NW-SE oriented shortening, subperpendicular to the margin, at least during the period spanning the Late Aptian to Late Cretaceous. In Zone 3 these phenomena were prolonged in time, extending into the Quaternary as revealed by the formation of local minibasins and thrusts in near-seafloor strata (Figs. 13, 14 and 17). In essence, these shallow thrusts are mainly concentrated east of structural highs H1 and H3, and are virtually absent in Zone 1.

8. Conclusions

Detailed mapping of the pre-salt succession in deep-water Santos Basin, and its overlying units, reveals an incomplete relationship between the syn-rift (pre-salt) topography and the styles of deformation of post-salt (Aptian) units. Based on the interpretation of a high quality 3D seismic volume, we demonstrate that:

a) Tighter folding and thrusting does not necessarily relate with the present-day structure at pre-salt level, nor necessarily coincide with the location of erosional features at the basal décollement surface.
b) This latter character hints at diachronous reactivation of pre-salt structures, and the existence of important tectonic movements after the main phase of salt deformation in SE Brazil. Evidence for reactivation of pre-salt structures include local pop-ups and normal faults revealing younger reverse offsets, gentle folding of half-grabens and grabens bound by reactivated normal faults, and horst and graben structures formed adjacently to main structural highs such as H2 and H4.
c) Observed discrepancies between pre-salt topography and thrust geometry result from important tectonic reactivation of parts of the studied margin.
d) The ramp gradients calculated for present-day pre-salt topography highlight the presence of pre-salt ramps and horsts that do not necessarily coincide with the regions of tighter folding and thrusting in the Aptian salt.

We propose that regions where erosion and truncation of pre-salt strata do not coincide necessarily with the highest ramp gradients observed at present, were uplifted and exposed sub-aerially before the deposition of Aptian salt – but can now be depressed areas in pre-salt successions, or part of horsts subsided after the Aptian. Locally, there is evidence for tectonic truncation below a moving mass of >2 km of evaporites. The noticeable increase in deformation towards the distal parts of the SE Brazil margin, where low-angle thrust nappes are ubiquitous on seismic data, is interpreted as resulting from combined gravitational gliding of salt from the northwest, and ridge push from the east and southeast. We also suggest that ridge push was responsible for a significant part of the salt deformation on the distal part of SE Brazil, and that this tectonic pulse had important effects on pre-salt reservoir and source rock compartmentalisation.

Acknowledgements

The authors acknowledge Petrobras for their permission to publish, together with F. Nepomuceno Filho and A.C.F Correa for the discussions held in Petrobras-London. We thank M. Moulin (Ifremer) for providing Fig. 4 in this paper. P. Kukla and two anonymous reviewers are acknowledged for their constructive comments.

References

Albertz, M., Beaumont, C., Ings, S.J., 2010. Geodynamic modeling of sedimentation-induced overpressure gravitational spreading and deformation of passive margin mobile shale basins. In: Wood, L. (Ed.), Shale Tectonics, 93. AAPG, Tulsa, pp. 29–62. Memoir vol.
Albertz, M., Ings, S.J., 2012. In: Alsop, G.I., Archer, S.G., Hartley, A.J., Grant, N.T., Hodgkinson, R. (Eds.), Some consequences of mechanical stratification in numerical models of passive-margin salt tectonics, 363. Geol. Soc. of London Spec. Pub, pp. 303–330.
Aslanian, D., Moulin, M., Olivet, J.-L., Unternehr, P., Matias, L., Bache, F., Rabineau, M., Nouzé, H., Klingelhoefer, F., Contrucci, I., Labails, C., 2009. Brazilian and African passive margins of the central segment of the South Atlantic Ocean: kinematic constraints. Tectonophysics 468, 98–112.
Bangs, N.L.B., Gulick, S.P.S., Shipley, T.H., 2006. Seamount subduction erosion in the Nankai Trough and its potential impact on the seismogenic zone. Geology 34, 701–704.
Bangs, N.L., Shipley, T.H., Gulick, S.P., Moore, G.F., Kuromoto, S., Nakamura, Y., 2004. Evolution of the Nankai Trough décollement from the trench into the seismogenic zone: inferences from three-dimensional seismic reflection imaging. Geology 32, 273–276.
Berger, P., Johnson, A.M., 1980. First-order analysis of deformation of a thrust sheet moving over a ramp. Tectonophysics 70, T9–T24.
Berger, P., Johnson, A.M., 1982. Folding of passive layers and forms of minor structures near terminations of blind thrust faults—application to the central Appalachian blind thrust. J. Str. Geol. 4, 343–353.
Bilotti, F., Shaw, J.H., 2005. Deep-water Niger Delta fold and thrust belt modeled as a critical-taper wedge: the influence of elevated basal fluid pressure on structural styles. AAPG Bull. 89, 1475–1491.
Brun, J.P., Fort, X., 2011. Salt tectonics at passive margins: geology versus models. Mar. Petr. Geol. 28, 1123–1145.
Brun, J.-P., Fort, X., 2012. Salt tectonics at passive margins: geology versus models - Reply. Mar. Petr. Geol. 37, 195–208.
Bueno, G.V., 2004. Event diachronism in the south Atlantic rift. Bol. Geociências Petrobras 14, 203–229.
Butler, R.W.H., 1987. Thrust sequences. J. Geol. Soc., London 144, 619–634.
Campan, A., 1995. Analyse cinématique de l'Atlantique Equatorial, implications sur l'évolution de l'Atlantique Sud et sur la frontière de plaque Amérique du Nord/Amérique du Sud. Univ. Pierre et Marie Curie, Paris. Paris VI (1995) 352 pp.
Contreras, J., Zühlke, R., Bowman, S., Bechstädt, Th, 2010. Seismic stratigraphy and subsidence analysis of the southern Brazilian margin (Campos, Santos and Pelotas basins). Mar. Petr. Geol. 27, 1952–1980.
Cotton, J.T., Koyi, H.A., 2000. Modeling of thrust fronts above ductile and frictional detachments: application to structures in the Salt Range and Potwar Plateau. Pak. Geol. Soc. Am. Bull. 112, 351–363.
Coward, M.P., 1983. Thrust tectonics, thin skinned or thick skinned, and the continuation of thrusts to deep in the crust. J. Struct. Geol. 5, 113–123.
Dahlen, F.A., 1990. Critical taper model of fold-and-Thrust belts and accretionary wedges. Ann. Rev. Earth Planet. Sci. 18, 55–99.
Davis, D., Suppe, J., Dahlen, F.A., 1983. Mechanics of fold-and-Thrust belts and accretionary wedges. J. Geophys. Res. 88, 1153–1172.
Davison, I., 2007. Geology and tectonics of the South Atlantic Brazilian salt basins. In: Ries, A.C., Butler, R.W.H., Graham, R.H. (Eds.), Deformation of the Continental Crust: the Legacy of Mike Coward, vol. 272. Geol. Soc., London, Sp. Pub, pp. 345–359.
Davison, I., Anderson, L., Nuttall, P., 2012. Salt deposition, loading and gravity drainage in the Campos and Santos salt basin. In: Alsop, G.I., Archer, S.G., Hartley, A.J., Grant, N.T., Hodgkinson, R. (Eds.), Salt Tectonics, Sediments and Prospectivity, vol. 363. Geol. Soc. London Sp. Publ, pp. 159–174.
Dooley, T.P., Jackson, M.P.A., Hudec, M.R., 2007. Initiation and growth of salt-based thrust belts on passive margins: results from physical models. Basin Res. 19, 165–177.
Dooley, T.P., Jackson, M.P.A., Jackson, C.A.-L., Hudec, M.R., Rodriguez, C.R., 2015. Enigmatic structures within salt walls of the Santos Basin-Part 2: mechanical explanation from physical modelling. J. Struct. Geol. 75, 163–187.
Duarte, C.S.L., Viana, A.R., 2007. Santos drift system: stratigraphic organization and implications for late cenozoic palaeocirculation in the Santos Basin, SW Atlantic Ocean. In: Viana, A., Rebesco, M. (Eds.), Economic and Palaeoceanographic Significance of Contourite Deposits, 276. Geol. Soc. Spec. Pub., London vol., pp. 171–198
Elliott, D., 1976. The motion of thrust sheets. J. Geophys. Res. 81, 949–963.
Fiduk, J.C., E.R. Brush, L.E. Anderson, P.B. Gibbs, Rowan M.G., 2004. Salt deformation, magmatism, and hydrocarbon prospectivity in the Espirito Santo Basin, offshore Brazil, in P.J. Post, D. Olson, K.T. Lyons, S.L. Palmes, P.F. Harison and N.C. Rosen, eds, Salt-sediment interactions and hydrocarbon prospectivity: Concepts, applications, and case studies for the 21st century: GCSSEPM 24th Annual Conference, p. 370–392.
Freitas, R.T.J., 2006. Ciclos deposicionais evaporíticos da bacia de Santos: uma análise ciclostratigráfica a partir de dados de 2 poços e de traços de sísmica. Unpublished MSc thesis. Instituto de Geociências, Universidade Federal do Rio Grande do Sul, Brazil.
Fuller, C.W., Willett, S.D., Brandon, M.T., 2006. Formation of forearc basins and their influence on subduction zone earthquakes. Geology 34, 65–68.
Ge, H., Jackson, Jackson, M.P.A., Vendeville, B.C., 1997. Kinematics and dynamics of

salt tectonic driven by progradation. AAPG Bull. 81, 398–423.
Gemmer, L., Beaumont, C., Ings, S.J., 2005. Dynamic modeling of passive margin salt tectonic: effects of water loading, sediment properties and sedimentation patterns. Basin Res. 17, 383–402.
Gradstein, F.M., Ogg, J.G., Smith, A.G., 2004. A Geologic Time Scale (Cambridge).
Gregory-Wodzicki, K.M., 2000. Uplift history of the central and Northern Andes: a review. GSA Bull. 112, 1091–1105.
Guerra, M., Underhill, 2012. Role of halokinesis in controlling structural styles and sediment dispersal in the Santos Basin, offshore Brazil. In: Alsop, G.I., Archer, S.G., Hartley, A.J., Grant, N.T., Hodgkinson, R. (Eds.), Salt Tectonics, Sediments and Prospectivity, vol. 363. Geol. Soc. London Sp. Publ., pp. 175–206
Henry, P., Lallemant, S., Nakamura, K., Tsunogai, U., Mazzotti, S., Kobayashi, K., 2002. Surface expression of fluid venting at the toe of the Nankai wedge and implications for flow paths. Mar. Geo 187, 119–143.
Jackson, C.A.-L., Rodriguez, C.R., Røtevatn, A., Bell, R.E., 2014. Geological and geophysical expression of a primary salt weld: an example from the Santos Basin, Brazil. Interpretation 2, SM77–SM89.
Jackson, C.A.-L., Jackson, M.P.A., Hudec, M.R., Rodriguez, C.R., 2015. Enigmatic structures within salt walls of the Santos Basin-Part 1: geometry and kinematics from 3D seismic reflection and well data. J. Struct. Geol. 75, 135–162.
Kodaira, S., Lidaka, T., Kato, A., Park, J.-O., Iwasaki, T., Kaneda, Y., 2004. High pore fluid pressure may cause silent slip in the nankai trough. Science 304, 1295–1298.
Koyi, H.A., Vendeville, B.C., 2003. The effect of décollement dip on geometry and kinematics of model accretionary wedges. J. Struct. Geol. 25, 1445–1450.
Lima, C., 2003. Ongoing Compression across South American Plate: observations, numerical modelling and some implications for petroleum geology. In: Ameen, M. (Ed.), Fracture and In-situ Stress Characterization of Hydrocarbon Reservoir, vol. 209. Geological Society, London, Special Publications, pp. 87–100.
Mégard, F., 1984. The Andean orogenic period and its major structures in central and northern Peru. J. Geol. Soc. Lond. 141, 893–900.
Mello, M.R., Telnaes, N., Maxwell, J.R., 1995. The Hydrocarbon Source Potential in the Brazilian Marginal Basins: a Geochemical and Paleoenvironmental Assessment. In: Huc, A.-Y. (Ed.), SG40: Paleogeography, Paleoclimate, Source Rocks. AAPG Studies in Geology 40, Tulsa.
Modica, C.J., Brush, E.R., 2004. Segmentation of an obliquely rifted margin, Campos and Santos basins, southeastern Brazil. AAPG Bull. 85, 1903–1924.
Mohriak, W.U., Macedo, J.M., Castelani, R.T., Rangel, H.D., Barros, A.Z.N., Latge, M.A.L., Ricci, J.A., Mizusaki, A.M.P., Szatmari, P., Demercian, L.S., Rizzo, J.G., Ayres, J.R., 1995. Salt tectonics and structureal styles in the deep-water province of the Cabo Frio Region, Rio de Janeiro, Brazil. In: Jackson, M.P.A., Roberts, D.G., Snelson, S., S. (Eds.), Salt Tectonics: a Global Perspective, vol. 65. AAPG Mem, pp. 273–304.
Mohriak, W.U., Nemcok, M., Enciso, G., 2008. South Atlantic divergent margin evolution: rift-borded uplift and salt tectonics in the basins of Southeastern Brazil. In: Pankhurst, R.J., Trouw, R.A.J., Brito Neves, B.B., de Wit, M.J. (Eds.), West Gondwana Pre-Cenozoic Correlations across the South Atlantic Region, vol. 294. Geol. Soc. London, Sp. Pub, pp. 365–398.
Moore, G.F., et al., 2001. New insights into deformation and fluid flow processes in the nankai trough accretionary prism: results of ocean drilling program leg 190. Geochem. Geophys. Geosyst 2, 1058.
Moreira, J.L.P., Carminatti, M., 2004. Sistemas Deposicionais de Talude e de Bacia no Eoceno da Bacia de Santos. Bol. Geoc. Petrobras 12, 73–87.
Moreira, J.L.P., Madeira, C.V., Gil, J.A., Machado, M.A.P., 2007. Santos Basin. Bul. Geoc. Petrobras 15, 531–549.
Morley, C.K., King, R., Hillis, R., Tingay, M., Backe, G., 2011. Deepwater fold and thrust belt classification, tectonics, structure and hydrocarbon prospectivity: a review. Earth Sci. Rev. 104, 41–91.
Moulin, M., Aslanian, D., Unternehr, P., 2010. A new starting point for the South and equatorial Atlantic Ocean. Earth-Sc. Rev. 98, 1–37.
Needham, H.D., Carré Daniel, Sibuet, J.-C., 1986. Carte bathymétrique de la ride de Walvis et du Bassin du Cap. Océan Atl. Sud. 1, 4382832. 4 maps, Ifremer.
Peacock, S.M., van Keken, P.E., Holloway, S.D., Hacker, B.R., Abers, G.A., Fergason, R.L., 2005. Thermal structure of the Costa Rica – Nicaragua subduction zone. Phys. Earth Plan. Int. 149, 187–200.
Quirk, D.G., Schodt, N., Lassen, B., Ings, S.J., Hsu, D., Hirsch, K.K., von Nicolai, C., 2012. Salt tectonics on passive margins: examples from Santos, Campos and Kwanza basins. In: Alsop, G.I., Archer, S.G., Hartley, A.J., Grant, N.T., Hodgkinson, R. (Eds.), Salt Tectonics, Sediments and Prospectivity, vol. 363. Geol. Soc. London Sp. Publ., pp. 207–244
Roberts, A.M., Yelding, G., 1991. Deformation Around Basin-margin Faults in the North Sea/mid-Norway Rift, vol. 56. Geol. Soc. London, Spec. Pub, pp. 61–78.
Rowan, M., Trudgill, B.D., Fiduk, J.C., 2000. Deep-water, salt-cored foldbelts: lessons from the Mississippi Fan and Perdido foldbelts, northern Gulf of Mexico. In: Webster, M., Talwani, M. (Eds.), Atlantic Rifts and Continental Margins, vol. 115. Am. Geophys. Union, Washington, pp. 173–191. Geophysical Monograph.
Rowan, M.G., Peel, F.J., Vendeville, B.C., 2004. Gravity-driven Foldbelts on Passive Margins, vol. 82. AAPG Memoir, pp. 157–182.
Rowan, M.G., Peel, F.J., Vendeville, B.C., Gaullier, V., 2012. Salt tectonics at passive margins: geology versus models - Discussion. Mar. Petr. Geol. 37, 184–194.
Rowan, M.G., 2014. Passive-margin salt basins: hyperextension, evaporite deposition, and salt tectonics. Bas. Res. 26, 154–182.
Ruh, J.B., Kaus, B.J.P., Burg, J.-P., 2012. Numerical investigation of deformation mechanisms in fold-and-thrust belts: influence of rheology of single and multiple décollements. Tectonics 31. http://dx.doi.org/10.1029/2011TC003047.
Sahabi, M., 1993. Modèle général de l'évolution de l'océan Indien, vol. 1. Univ. de Bretagne Occidentale, Brest et 243 pp. vol. 2187 pp.
Soares, D.M., Alves, T.M., Terrinha, P., 2012. The breakup sequence and associated lithospheric breakup surface: their significance in the context of rifted continental margins (West Iberia and Newfoundland margins, North Atlantic). Earth Plan. Sc. Lett. 355–356, 311–326.
Tavani, S., Storti, F., Lacombe, O., Corredetti, A., Muñoz, J.A., Mazzoli, S., 2015. A review of deformation pattern templates in foreland basin systems and fold-and-thrust belts: implications for the state of stress in the frontal regions of thrust wedges. Earth-Sc. Rev. 141, 82–104.
Trusheim, F., 1957. Über Halokinese und ihre Bedeutung für die strukturelle Entwicklung Norddcutschlands. Z. Deutch. Geol. Ges. 198, 111–151.
Trusheim, F., 1960. Mechanism of salt migration in northern Germany. AAPG Bull. 44, 1519–1540.
Weijermars, R., Jackson, M.P.A., Vendeville, B., 1993. Rheological and tectonic modeling of salt provinces. Tectonophysics 217, 143–174.
Weijermars, R., Jackson, M.P.A., Dooley, T.P., 2014. Quantifying drag on wellbore casings in moving salt sheets. Geophys. J. Int. 198, 965–977.